于太极,王璞珺,高有峰等. 2024. 松辽盆地西缘突泉地区晚侏罗世过铝质流纹岩和英云闪长玢岩的发现:从蒙古-鄂霍茨克洋闭合到陆陆碰撞的地质记录. 岩石学报,40(01): 159 - 177, doi: 10.18654/1000 - 0569/2024.01.09

松辽盆地西缘突泉地区晚侏罗世过铝质流纹岩和英云闪长玢岩的发现:从蒙古-鄂霍茨克洋闭合到陆陆碰撞的地质记录*

于太极[1,2] 王璞珺[2**] 高有峰[2,3] 张艳[2] 陈崇阳[4]

YU TaiJi[1,2], WANG PuJun[2**], GAO YouFeng[2,3], ZHANG Yan[2] and CHEN ChongYang[4]

1. 辽宁工程技术大学安全科学与工程学院,葫芦岛 125105
2. 吉林大学地球科学学院,长春 130061
3. 吉林大学古生物学与地层研究中心,长春 130026
4. 吉林师范大学旅游与地理科学学院,四平 136000

1. *College of Safety Science and Engineering, Liaoning Technical University, Huludao* 125105, *China*
2. *College of Earth Sciences, Jilin University, Changchun* 130061, *China*
3. *Research Center of Paleontology and Stratigraphy, Jilin University, Changchun* 130026, *China*
4. *College of Tourism and Geographic Sciences, Jilin Normal University, Siping* 136000, *China*

2023-06-25 收稿, 2023-11-02 改回.

Yu TJ, Wang PJ, Gao YF, Zhang Y and Chen CY. 2024. Discovery of the Late Jurassic peraluminous rhyolites and tonalite porphyrites in the Tuquan area along the western margin of the Songliao Basin: Geological records from closure of the Mongol-Okhotsk Ocean to continental collision between the Siberian plate and the Erguna-Songliao block. *Acta Petrologica Sinica*, 40(1): 159 - 177, doi: 10.18654/1000-0569/2024.01.09

Abstract The southeastward subduction of the Mongol-Okhotsk Ocean, oceanic closure, and continental collision were important regional tectonic events in the Late Mesozoic of Northeast Asia. They are closely related to magmatic activity, metamorphism, basin formation and orogeny in the area. Accurately defining the spatiotemporal range of the interrelated geological processes of the above three events is a prerequisite for understanding the tectonics of the region in the Late Mesozoic. However, it is difficult to conduct this kind of investigation as it is difficult to find suitable geological records related to these events. We discovered peraluminous rhyolites and tonalite porphyrites in the Tuquan area along the western margin of the Songliao Basin. These samples are probably related to the oceanic closure and continental collision. The zircon LA-ICP-MS U-Pb dating results show that their crystallization ages are 156 ± 1Ma and 155 ± 1Ma, respectively, indicating they are the products of Late Jurassic magmatic events. They are calc-alkaline peraluminous rocks with high aluminum saturation index A/CNK (1.32 ~ 2.13) and low content of $MgO + FeO^T$ (0.96% ~ 3.37%) and low ratio of FeO^T/MgO (2.84 ~ 5.02). Thin-section work shows that they contain high aluminum minerals such as sericite. Corundum molecules (3.77% ~ 9.65%) appear in CIPW standard mineral calculation, and these rhyolites and tonalite porphyrites are mapped in the geochemical diagrams related to the S-I-M-A classification scheme of granites. These results show the characteristics of S-type granites. The low ratios of Rb/Sr (0.35 ~ 0.55) and Rb/Ba (0.08 ~ 0.26) of rhyolites and tonalite porphyrites indicate that the primary magma of rhyolites and tonalite porphyrites were originated from poor argillaceous arenaceous rocks. Zircon saturation temperature calculation shows that the magmatic crystallization temperatures of rhyolites and tonalite porphyrites range from 837℃ to 876℃, and the samples have high ratio of Al_2O_3/TiO_2 (38.41 ~ 61.36), these temperatures are lower than the formation temperature of A-type granite (900℃). These rhyolites and tonalite porphyrites are richen in large ion lithophile elements such as Rb, Ba, K, and lack high

* 本文受国家自然科学基金项目(41790453、41472304、42102129、41972313)和国家重点研发计划(2019YFC0605402)联合资助.

第一作者简介: 于太极,男,1988 年生,讲师,从事岩石学和构造地质学研究,E-mail: yutj1988@126.com

** **通讯作者**:王璞珺,男,1959 年生,教授,博士生导师,主要从事盆地地质和火山岩储层、沉积学和火山学的研究与教学,E-mail: wangpj@jlu.edu.cn

field strength elements such as Nb, Ta, P, Ti. They also show low contents of Y (5.29×10^{-6} ~ 19.75×10^{-6}), Nb (7.44×10^{-6} ~ 8.50×10^{-6}), Sr (60.6×10^{-6} ~ 154.9×10^{-6}) and Yb (0.53×10^{-6} ~ 2.40×10^{-6}), showing arc magmatic properties. In the R1-R2 major element tectonic discrimination diagram, the samples are mainly projected within the range of collisional and orogenic periods. The Nb-Y diagram shows that the samples are dotted in volcanic arcs and syn-collision granites. The Rb/10-Hf-Ta×3 diagram shows that the samples are located in the regions of volcanic arcs and collision type granite. The Sr-Yb diagrams indicate that rhyolites and tonalite porphyrites were formed in the stage of crustal thickening. The tectonic discrimination for the rhyolites and tonalite porphyrites in the Tuquan area is suggested that the Late Jurassic in the area was a period of the volcanic arc and continental crust collision environments. It implies that their formation is related to oceanic crust subduction and continental collision during the closure process of the Mongol-Okhotsk Ocean. The ratio of rhyolites $(La/Yb)_N$ range from 6.62 to 8.77, indicating a depth of 40 ~ 46km in the source area. The ratio of tonalite porphyrites $(La/Yb)_N$ range from 7.93 to 13.39, indicating a depth of 44 ~ 55km in the source area. These results indicate that a continuous thickening process of the crust at 156 ± 1Ma to 155 ± 1Ma. These characteristics of rhyolites and tonalite porphyrites provide key igneous rock evidence for evolution from oceanic subduction to continental collision. Combined with the regional geological data, the tectonic-magmatic evolution model of the Mongol-Okhotsk Ocean from the subduction and closure to the continental collision is constructed. In this paper, the influence range of the Mongol-Okhotsk Ocean tectonic system reached the Tuquan area in the western margin of the Songliao Basin, the Mongol-Okhotsk Ocean was closed at 156 ± 1Ma, and the study area at 155 ± 1Ma was at the stage of continental collision and crust thickening after ocean closure.

Key words Songliao Basin; Rhyolite; Tonalite porphyrite; Peraluminous; Late Jurassic; Closure of the Mongol-Okhotsk Ocean; Collision between the Siberian plate and Erguna-Songliao block

摘 要 蒙古-鄂霍茨克洋南向俯冲、大洋闭合和陆-陆碰撞是东北亚地区晚中生代的重要区域构造事件,它与本区的岩浆活动、变质作用、成盆和造山作用都密切相关。准确界定洋壳俯冲、大洋闭合和陆-陆碰撞这三个相互关联地质过程的时空范围是客观认识区域构造演化的前提。然而,这项研究通常难以进行,因为很难找到与之相关的合适的地质记录。作者在松辽盆地西缘突泉地区发现从大洋闭合到陆-陆碰撞相关的过铝质流纹岩和英云闪长玢岩,锆石 LA-ICP-MS U-Pb 定年结果显示其结晶年龄分别为 156 ± 1Ma 和 155 ± 1Ma,系晚侏罗世岩浆事件产物。流纹岩和英云闪长玢岩为钙碱性过铝质岩石,具有较高的铝饱和指数 A/CNK(1.32 ~ 2.13),较低的 $MgO+FeO^T$ 含量(0.96% ~ 3.37%)和 FeO^T/MgO 比值(2.84 ~ 5.02),岩矿鉴定表明它们含绢云母等原生和次生高铝矿物,在 CIPW 标准矿物计算中出现刚玉分子(3.77% ~ 9.65%),结合流纹岩和英云闪长玢岩在花岗岩的 S-I-M-A 型分类方案相关地球化学图解投影结果,综合表明它们具有过铝质 S 型花岗岩特征。流纹岩和英云闪长玢岩具有较低的 Rb/Sr(0.35 ~ 0.55)、Rb/Ba(0.08 ~ 0.26)和 Al_2O_3/TiO_2(38.41 ~ 61.36)比值,表明其原始岩浆源于杂砂岩部分熔融。锆石饱和温度计算表明这两类岩石的岩浆形成温度在 837 ~ 876℃之间,低于 A 型花岗岩岩浆形成温度(900℃)。两类岩石富集 Rb、Ba、K 等大离子亲石元素,亏损 Nb、Ta、P、Ti 等高场强元素,具有较低的 Y(5.29×10^{-6} ~ 19.75×10^{-6})、Nb(7.44×10^{-6} ~ 8.50×10^{-6})、Sr(60.6×10^{-6} ~ 154.9×10^{-6})和 Yb(0.53×10^{-6} ~ 2.40×10^{-6})含量,具有弧岩浆属性。在 Y-Nb 图解中流纹岩和英云闪长玢岩投点在火山弧和同碰撞型花岗岩区域内;在 Rb/10-Hf-Ta×3 图解中投点在火山弧和碰撞型花岗岩区域内;在 R1-R2 构造判别图解中样品投点在同碰撞和造山期区域内;在 Sr-Yb 图解中样品投点在地壳加厚区域内。结合全球典型俯冲岛弧和同碰撞酸性岩地球化学特征和同时期本区域岩浆岩成因,表明流纹岩和英云闪长玢岩形成于洋壳俯冲和陆-陆碰撞转换背景,暗示其形成与蒙古-鄂霍茨克茨洋闭合和陆-陆碰撞作用有关。流纹岩 $(La/Yb)_N$ 值为 6.62 ~ 8.77,指示源区起源深度为 40 ~ 46km,英云闪长玢岩 $(La/Yb)_N$ 值为 7.93 ~ 13.39,指示源区起源深度为 44 ~ 55km,表明在 156 ± 1Ma ~ 155 ± 1Ma 地壳处于持续加厚过程。结合区域地质资料,构建了蒙古-鄂霍茨克洋从俯冲闭合到陆-陆碰撞的构造-岩浆演化模型。本文认为蒙古-鄂霍茨克构造体系的影响范围到达了松辽盆地西缘突泉地区,156 ± 1Ma ~ 155 ± 1Ma 研究区处于大洋闭合到陆-陆碰撞转换阶段。

关键词 松辽盆地;流纹岩;英云闪长玢岩;过铝质;晚侏罗世;蒙古-鄂霍茨克洋闭合;陆-陆碰撞

中图法分类号 P588.134;P588.141; P597.3

过铝质花岗岩在全球造山带中广泛分布(Sylvester, 1998; Barbarin, 1999; Chappell and White, 2001),可形成于俯冲(Chen *et al.*, 2014)、活动大陆边缘和陆-陆碰撞等构造环境(Finger *et al.*, 1997; Sylvester, 1998)。一般认为过铝质花岗岩是陆壳富铝质沉积物部分熔融形成的(Le Fort *et al.*, 1987; Kapp *et al.*, 2002),其形成机制和热量来源包括板片断离(Xu *et al.*, 2022)、陆内俯冲(邓晋福等, 1994)、陆-陆碰撞过程中地壳的堆叠加厚(Barbarin, 1996)、构造减压(Gerdes *et al.*, 2002; 张宏飞等, 2005)和幔源物质的底侵(Elburg, 1996)等。因此过铝质花岗岩的矿物学和地球化学特征对研究陆壳部分熔融时源区物质组成、形成温度、热量来源和地球动力学背景具有重要作用。

中国东北地区位于中亚造山带东段,从古生代到新生代经历了复杂的演化过程,尤其是中生代以来经历了蒙古-鄂霍茨克洋闭合和古太平洋俯冲的叠加与改造(Wang *et al.*, 2006, 2016; Zhang *et al.*, 2010, 2011)。近年来,为揭示蒙古-鄂霍茨克洋闭合和古太平洋俯冲对东北地区影响的时间及空间范围,大量学者对东北地区中生代火成岩的年代学和

地球化学进行研究（李宇等，2015；Ouyang *et al.*，2015；Tang *et al.*，2015；Guo *et al.*，2015；Wang *et al.*，2019；Huang *et al.*，2021；Ji *et al.*，2021），其研究范围主要集中在额尔古纳地块、兴安地块和佳木斯地块，普遍认为额尔古纳地块和兴安地块岩浆活动与蒙古-鄂霍茨克洋的闭合有关（Xu *et al.*，2013；Ouyang *et al.*，2015；Wang *et al.*，2015；Li *et al.*，2017），松辽盆地东部和佳木斯地块的岩浆活动与古太平洋板块的俯冲有关（Guo *et al.*，2015；Huang *et al.*，2021；Ji *et al.*，2021）。松辽盆地西缘相对远离蒙古-鄂霍茨克缝合带和古太平洋俯冲带，针对性研究较少，这限制了对东北地区中生代蒙古-鄂霍茨克洋闭合和古太平洋俯冲构造演化的认识。而且关于蒙古-鄂霍茨克洋的闭合时间仍存在分歧，基于古地磁数据分析认为闭合时间有以下几种观点：（1）三叠纪到晚侏罗世闭合（Şengör and Natal'in，1996；Kravchinsky *et al.*，2002）；（2）早、中侏罗世闭合（Zorin，1999；Parfenov *et al.*，2001）；（3）中侏罗世闭合（Kirillova，2003；Tomurtogoo *et al.*，2005；李宇等，2015）；（4）早白垩世闭合（Enkin *et al.*，1992；Halim *et al.*，1998；Ren *et al.*，2016）。近年来蒙古-鄂霍茨克缝合带及邻区岩石学和地球化学的研究工作日趋增多，与蒙古-鄂霍茨克洋俯冲相关和陆-陆碰撞后伸展相关的岩浆岩年代学和地球化学研究为蒙古-鄂霍茨克构造体系演化提供了更多的依据，但与大洋闭合和陆-陆碰撞直接相关的过铝质 S 型花岗岩缺少明确证据报道。

本文报道了松辽盆地西缘突泉地区发现的晚侏罗世过铝质流纹岩和英云闪长玢岩的岩相特征、锆石 U-Pb 年龄和全岩地球化学数据，以探讨其岩石成因、岩浆源区和构造背景，为蒙古-鄂霍次克洋闭合到陆-陆碰撞的时空范围提供合理的约束。

1 地质背景与样品描述

中国东北地区位于中亚造山带东部，西北部经蒙古-鄂霍茨克缝合带与西伯利亚克拉通相连，南部经西拉木伦-长春-延吉缝合带与华北克拉通相连，东部与古太平洋板块相接，其组成单元从西北到东南可分为额尔古纳地块、兴安地块、松辽地块和佳木斯地块。这些块体被新林-喜桂图缝合带、贺根山-黑河缝合带、牡丹江-依兰缝合带分隔（图 1a；Liu *et al.*，2017）。突泉地区位于松辽盆地西缘，研究区主要为侏罗系和下白垩统地层，从下至上发育沉积岩、酸性火山岩和中基性火山岩，并发育一系列不定向展布的侵入岩岩体和定向排列的脉岩。

本次研究的流纹岩（D11、D12、D13 和 D14）出露在突泉地区西部公路旁剖面（N45°22′49.6″、E121°26′16.9″）（图 1b）。流纹岩呈层状产出，角度不整合于中侏罗世砂岩之上，二者均被早白垩世煌斑岩岩脉侵入（图 2a-c）。英云闪长玢岩（MN6、MN7、MN10、MN11 和 MN12）出露在突泉地区东南部牝牛海露天煤矿中，该煤矿煤层发育在中侏罗统地层中，上部为第四系（N45°12′10.2″、E121°48′11.2″）（图 1b）。英云闪长玢岩为中侏罗统沉积地层中一系列小而密集的浅层侵入体。英云闪长玢岩以岩脉的形式出现，厚度约为 2 ~ 5m，呈北东向分布，与中侏罗世砂岩有明显的接触边界（图 2e）。

表 1 突泉地区流纹岩和英云闪长玢岩显微镜下矿物组成和含量

Table 1 Mineral composition and characteristics of rhyolite and tonalite porphyrite under microscope in Tuquan area

样品号	岩性	石英	钾长石	斜长石	绢云母	副矿物
		主要矿物含量（vol%）				
D11	流纹岩	65	20	10	4	1
D12		65	20	10	4	1
D13		60	20	15	4	1
D14		65	15	15	4	1
MN6	英云闪长玢岩	20	5	65	9	1
MN7		25	5	60	9	1
MN10		25	5	65	4	1
MN11		20	5	70	4	1
MN12		25	5	65	4	1

流纹岩和英云闪长玢岩的岩石矿物含量（表 1）和特征如下：

流纹岩，呈土黄色，块状构造，具有斑状结构，斑晶为斜长石（~10%）、钾长石（~20%）、石英（~5%），基质由隐晶状长英质矿物组成（~60%），并含有绢云母和副矿物（~5%）。斜长石斑晶呈半自形板柱状，无序排列，粒度 0.5 ~ 1.5mm，晶体中具卡纳复合双晶，其消光角小，为钠更长石或钠长石，部分被熔蚀成港湾状。少见斜长石晶屑和安山岩岩屑（~5%），斜长石晶屑呈次棱角状或者棱角状。安山岩岩屑中见针状斜长石，呈微晶状，紧密平行排列。钾长石斑晶呈半自形柱状，粒度 0.2 ~ 1mm，为正长石和微斜长石，呈平行消光，其边缘有熔蚀。绢云母呈自形-半自形片状，发育在矿物缝隙或者斜长石中（图 2c）。

英云闪长玢岩，呈灰白色，半自形粒状构造，具斑状结构，主要矿物为斜长石（~65%）、钾长石（~5%）、石英（~25%）、绢云母（~10%）。斜长石呈半自形长条状，微定向排列，粒度 0.1 ~ 0.5mm。钾长石呈半自形，粒度 0.1 ~ 0.2mm。石英呈自形粒状和隐晶状。原生矿物绢云母呈半自形细小鳞片状分布，干涉色鲜艳多在二到三级；次生矿物绢云母为斜长石绢云母化形成，颜色为淡黄色（图 2f）。

2 分析方法

2.1 锆石 U-Pb 定年

对样品的锆石挑选、制靶和阴极发光图像采集在河北廊坊地质调查研究院完成。采用常规方法将样品粉碎至 100

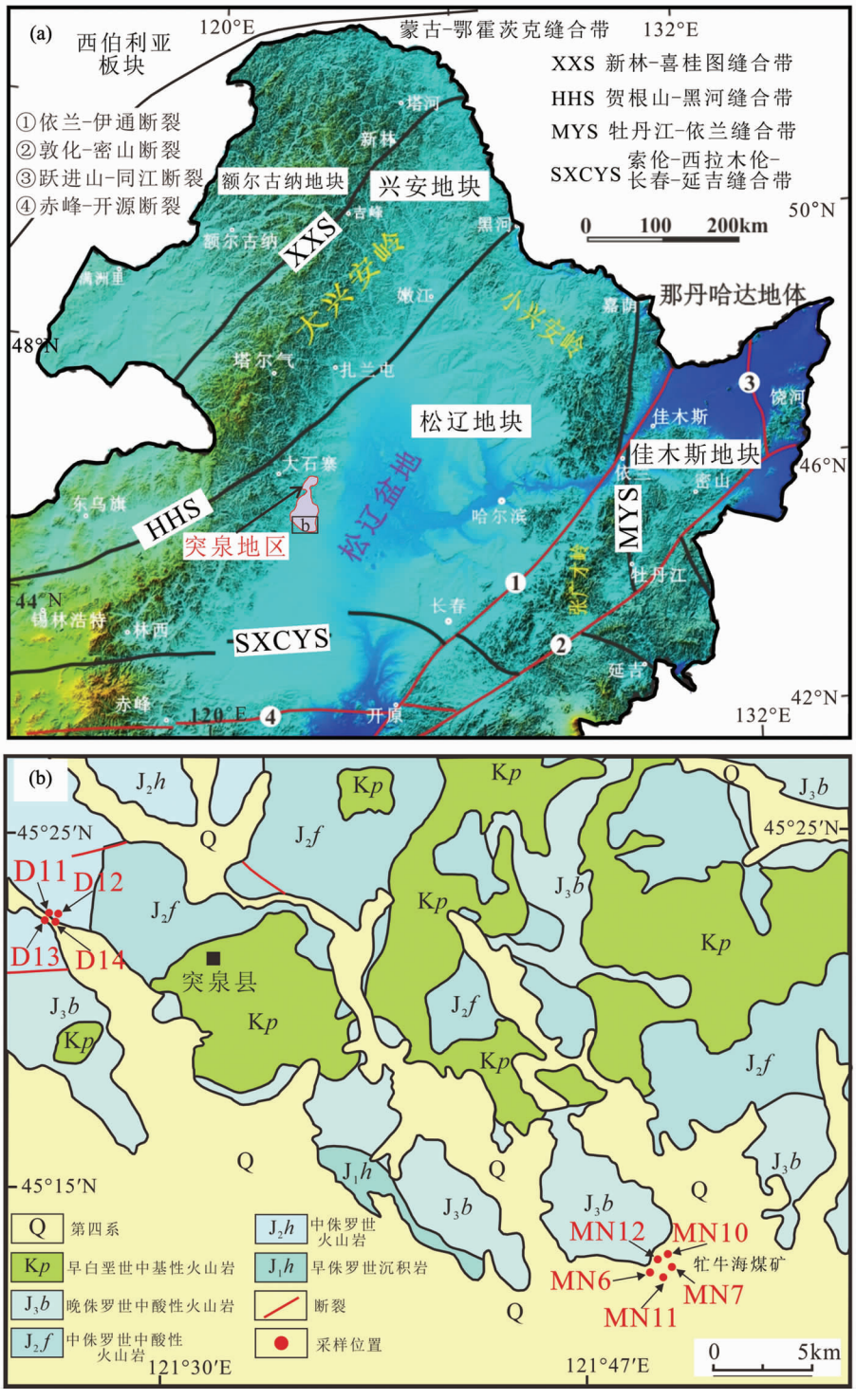

图 1 中国东北地区构造简图(a,据 Liu *et al.*, 2017)和突泉地区地质简图(b,据吉林省地质矿产局, 1988)

Fig. 1 Tectonic subdivisions of northeastern China and the location of the Tuquan area (a, modified after Liu *et al.*, 2017) and simplified geological map of the Tuquan area showing sample locations (b, modified after BGMRJ, 1988)

目,经浮选、磁力分选后,利用双目镜挑选出晶形完好、长宽比例适中、透明度和色泽度好、具有柱面特征的锆石颗粒。然后将其粘贴在环氧树脂中,制成锆石靶,再进行打磨和抛光直至锆石新鲜的核部暴露出来。完成样品制靶后,对锆石进行透射光和反射光显微图像采集,依据阴极发光和透反射照片选择最佳的锆石位置进行 U-Pb 定年。

锆石 LA-ICP-MS U-Pb 年龄分析在中国地质大学(武汉)地质过程与矿产资源国家重点实验室和吉林大学东北亚矿

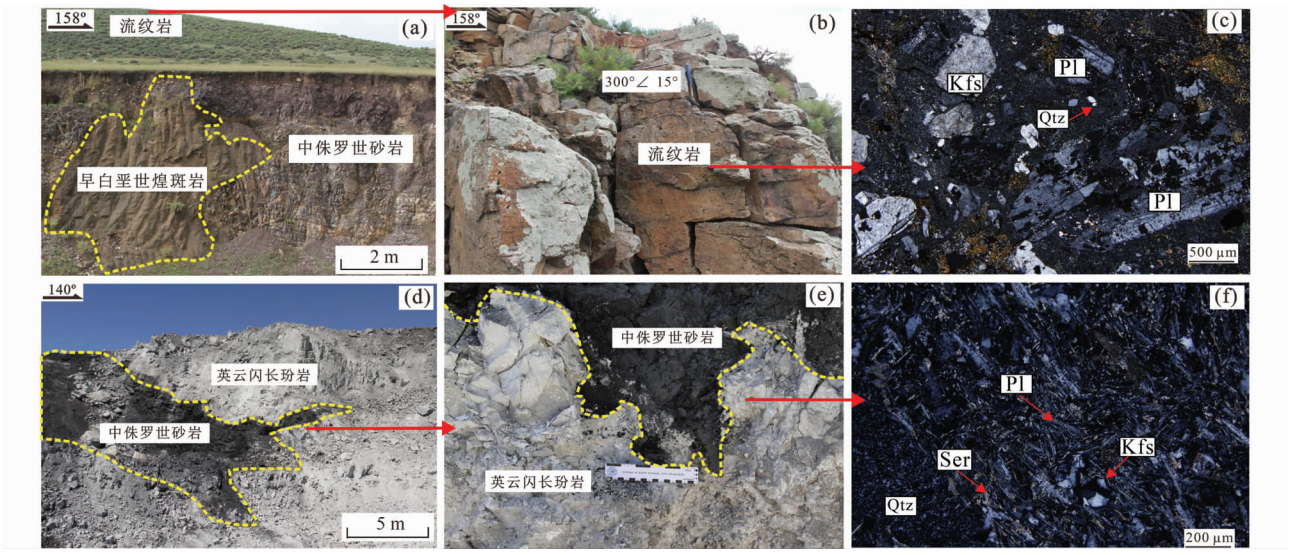

图 2　突泉地区晚侏罗世流纹岩和英云闪长玢岩野外露头照片和显微镜下照片

(a)流纹岩角度不整合在中侏罗世砂岩之上，二者被煌斑岩侵入；(b)流纹岩呈层状发育；(c)流纹岩正交偏光照片，见石英、钾长石和斜长石；(d)英云闪长玢岩侵入到中侏罗世砂岩；(e)英云闪长玢岩与围岩的接触局部照片；(f)英云闪长玢岩正交偏光照片，见绢云母．Kfs-钾长石；Pl-斜长石；Qtz-石英；Ser-绢云母

Fig. 2　Field photographs and photomicrographs of the rhyolites and tonalite porphyrites in the Tuquan area

(a) the rhyolite was in unconformable contact with the Mid-Jurassic sandstones, which were intruded by lamprophyre; (b) the rhyolite was developed in layers; (c) micro photographs of the rhyolite; (d) the contact between tonalite porphyry and the surrounding rock; (e) the local photograph of the contact between tonalite porphyry and the surrounding rock; (f) micro photographs of the tonalite porphyry. Kfs-kfeldspar; Pl-plagioclase; Qtz-quartz; Ser-sericite

产资源评价重点实验室完成，两所实验室的激光剥蚀系统均为 GeoLas 2005，分析测试仪器 ICP-MS 型号均为 Agilent 7500a 型，激光剥蚀斑束的直径为 32μm，剥蚀深度为 20～40μm，实验过程中采用哈佛大学国际标准锆石 91500（≈1064Ma）作为校正外标样品，GJ-1（≈599Ma）作为监控样品，进行同位素分馏校正，锆石的微量元素含量采用美国国家标准技术研究院研制的人工合成硅酸盐玻璃标准物质 NIST 610 作为外标样品，Si 作为内标进行计算，每个样品分析数据包括 15～20s 空白信号和 40～50s 样品剥蚀信号。对样品信号的选择、仪器灵敏度漂移校正、元素含量及 U-Pb 同位素数值、锆石年龄计算等分析数据的离线处理均采用软件 ICPMSDataCal（Ver. 6.7；Liu *et al.*，2010）完成。普通 Pb 校正采用 Andersen（2002）方法，样品的 U-Pb 年龄谐和图绘制和加权平均年龄计算采用国际标准程序 Isoplot（Ver. 3.00；Ludwig，2003）完成。同位素比值和年龄误差为 1σ 水平，置信水平为 95%，加权平均年龄采用$^{206}Pb/^{238}U$ 年龄。

2.2　主量元素和微量元素

本研究样品的全岩主、微量元素分析测试均在吉林大学东北亚矿产资源评价重点实验室完成。主量元素采用 X 射线荧光光谱分析（XRF；Rigaku ZSX Primu Ⅱ型），通过容量法测定 FeO 含量，通过重量法测定 LOI 值。采用 Agilent 7500a 型 ICP-MS 分析微量元素。通过美国地质调查局标准物质 BHVO-1、BCR-2 和 AGV-1 以及中国国家标准物质 GSR-1 的对比分析表明，主量元素分析精度和准确度优于 1%，微量元素分析精度和准确度优于 5%。

3　分析结果

3.1　锆石特征及 U-Pb 年代学

本文对 1 件流纹岩样品（D12）和 1 件英云闪长玢岩样品（MN7）进行锆石 LA-ICP-MS U-Pb 定年。锆石晶体选取无色透明，晶形以长柱状为主，锆石粒径介于 87～142μm，长宽比 1∶1～3∶1（图 3、表 2）。锆石晶体形态比较完整，边部具有清晰的振荡环带特征，锆石 Th/U 比值大于 0.2（图 3、表 2），属于岩浆锆石（Hoskin and Schaltegger，2003）。

流纹岩样品（D12）39 颗锆石分析测试点均落在$^{206}Pb/^{238}U$和$^{207}Pb/^{235}U$ 谐和线上，表明谐和性较好，锆石在形成后其 U-Pb 体系一直保持封闭状态。单颗粒锆石的$^{206}Pb/^{238}U$ 年龄值介于 152.1±1.6Ma～161.0±1.8Ma 之间，加权平均年龄为 156±1Ma（MSWD=1.8），指示流纹岩形成于晚侏罗世（图 3a、表 2）。

英云闪长玢岩样品（MN7）37 颗锆石分析测试点均落在$^{206}Pb/^{238}U$ 和$^{207}Pb/^{235}U$ 谐和线上，表明谐和性较好，锆石在形成后其 U-Pb 体系一直保持封闭状态。单颗粒锆石的$^{206}Pb/^{238}U$ 年龄值介于 147.4±3.9Ma～163.6±4.5Ma 之间，加权平均年龄为 155±1Ma（MSWD=1.3），指示英云闪长玢

表 2 突泉地区流纹岩和英云闪长玢岩锆石 LA-ICP-MS U-Pb 定年结果

Table 2 LA-ICP-MS U-Pb isotopic data for zircons from the the rhyolites and tonalite porphyrites in the Tuquan area

测点号	含量($\times10^{-6}$)			Th/U	同位素比值						年龄(Ma)					
	Pb	Th	U		$\frac{^{207}Pb}{^{206}Pb}$	1σ	$\frac{^{207}Pb}{^{235}U}$	1σ	$\frac{^{206}Pb}{^{238}U}$	1σ	$\frac{^{207}Pb}{^{206}Pb}$	1σ	$\frac{^{207}Pb}{^{235}U}$	1σ	$\frac{^{206}Pb}{^{238}U}$	1σ
D12,流纹岩																
-1	31	200	422	0.47	0.05430	0.0023	0.1786	0.0072	0.0241	0.0003	383.4	96.3	166.8	6.2	153.3	1.6
-2	15	97	231	0.42	0.04840	0.0025	0.1596	0.0076	0.024	0.0003	120.5	118.5	150.3	6.6	153.0	2.1
-3	36	191	947	0.20	0.04930	0.0015	0.1628	0.0047	0.024	0.0002	161.2	65.7	153.2	4.1	152.6	1.3
-4	31	199	403	0.49	0.05480	0.0022	0.1825	0.0069	0.0245	0.0003	466.7	95.4	170.2	5.9	155.8	1.9
-5	20	124	307	0.40	0.05150	0.0025	0.1739	0.0084	0.0244	0.0003	261.2	117.6	162.8	7.3	155.6	2.0
-6	50	390	505	0.77	0.04860	0.0016	0.1603	0.0054	0.0239	0.0003	131.6	87.0	151.0	4.8	152.1	1.6
-7	15	95	235	0.41	0.05330	0.003	0.1776	0.0086	0.0246	0.0004	342.7	124.1	166.0	7.4	156.6	2.6
-8	33	256	391	0.65	0.04890	0.0019	0.1604	0.0061	0.0239	0.0003	142.7	92.6	151.1	5.3	152.5	1.9
-9	16	106	231	0.46	0.05280	0.0028	0.1719	0.0084	0.0243	0.0004	320.4	118.5	161.0	7.3	154.9	2.5
-10	25	157	318	0.49	0.05630	0.0025	0.187	0.008	0.0243	0.0003	464.9	100.0	174.0	6.8	154.8	2.0
-11	18	108	262	0.41	0.05550	0.0027	0.1856	0.0085	0.0246	0.0003	435.2	109.3	172.8	7.3	156.8	2.0
-12	38	274	556	0.49	0.04960	0.0018	0.1634	0.006	0.0241	0.0003	176.0	83.3	153.7	5.2	153.6	1.8
-13	16	94	244	0.39	0.05150	0.0029	0.1705	0.0092	0.0245	0.0004	264.9	95.4	159.8	8.0	155.7	2.2
-14	13	71	206	0.34	0.05080	0.0028	0.1691	0.0084	0.0248	0.0004	235.3	137.0	158.6	7.3	158.0	2.3
-15	29	230	339	0.68	0.05250	0.0026	0.179	0.0088	0.0253	0.0004	309.3	100.9	167.2	7.6	160.8	2.4
-16	21	134	323	0.41	0.05080	0.0024	0.1693	0.0077	0.0245	0.0003	235.3	111.1	158.8	6.7	156.0	1.8
-17	27	180	384	0.47	0.04980	0.0021	0.1647	0.0069	0.0242	0.0003	187.1	100.0	154.8	6.1	154.0	1.8
-18	51	388	557	0.70	0.04920	0.0017	0.165	0.0058	0.0243	0.0003	166.8	77.8	155.0	5.1	154.7	1.6
-19	29	211	340	0.62	0.05150	0.0024	0.1742	0.0078	0.0247	0.0003	261.2	105.5	163.1	6.8	157.2	1.7
-20	27	160	385	0.42	0.05520	0.0023	0.1911	0.0072	0.0252	0.0003	433.4	92.6	177.6	6.2	160.7	1.9
-21	13	84	206	0.41	0.05160	0.0033	0.1704	0.0096	0.0245	0.0004	333.4	148.1	159.8	8.3	155.9	2.4
-22	24	164	305	0.54	0.05000	0.0025	0.1748	0.0081	0.0253	0.0003	194.5	116.7	163.6	7.0	161.0	1.8
-23	17	117	295	0.40	0.04990	0.0027	0.1675	0.0084	0.0249	0.0003	190.8	159.2	157.2	7.3	158.3	2.2
-24	49	373	496	0.75	0.05120	0.002	0.1742	0.0064	0.0249	0.0003	250.1	90.7	163.0	5.5	158.5	1.7
-25	13	89	203	0.44	0.05000	0.0031	0.165	0.0093	0.0245	0.0003	198.2	141.7	155.1	8.1	156.0	2.2
-26	16	115	243	0.48	0.05550	0.0027	0.1856	0.0081	0.0246	0.0003	435.2	109.3	172.8	7.0	156.8	2.0
-27	20	125	325	0.38	0.05330	0.0024	0.1836	0.0078	0.0251	0.0003	342.7	96.3	171.1	6.7	160.0	1.9
-28	19	135	290	0.47	0.05060	0.0027	0.1637	0.0078	0.024	0.0003	233.4	130.5	153.9	6.8	152.7	1.9
-29	28	173	391	0.44	0.05450	0.0023	0.1845	0.008	0.0244	0.0003	390.8	94.4	171.9	6.8	155.6	2.0
-30	35	214	567	0.38	0.04890	0.0018	0.1673	0.0058	0.0249	0.0003	142.7	82.4	157.1	5.0	158.3	1.6
-31	21	158	290	0.54	0.05020	0.0029	0.1689	0.0093	0.0244	0.0003	211.2	131.5	158.4	8.1	155.6	2.0
-32	32	240	370	0.65	0.05020	0.0023	0.1725	0.0077	0.0249	0.0003	211.2	106.5	161.6	6.7	158.6	1.8
-33	40	306	443	0.69	0.04890	0.0018	0.1682	0.0062	0.0249	0.0003	142.7	83.3	157.9	5.4	158.7	1.8
-34	30	235	360	0.65	0.04890	0.0024	0.1656	0.0077	0.0247	0.0003	146.4	114.8	155.6	6.7	157.0	1.9
-35	14	94	246	0.38	0.04960	0.0025	0.1659	0.0076	0.0246	0.0003	176.0	123.1	155.8	6.6	156.8	1.9
-36	16	106	279	0.38	0.04930	0.0025	0.1653	0.0078	0.0246	0.0003	164.9	149.1	155.3	6.8	156.6	2.0
-37	35	280	351	0.80	0.04940	0.0021	0.1682	0.007	0.0246	0.0003	168.6	100.0	157.9	6.1	156.6	1.7
-38	25	174	316	0.55	0.05110	0.0021	0.1727	0.007	0.0245	0.0003	242.7	99.1	161.8	6.1	156.2	1.8
-39	36	255	418	0.61	0.05440	0.0021	0.1891	0.007	0.0253	0.0003	387.1	87.0	175.9	6.0	160.8	1.8
MN7,英云闪长玢岩																
-1	4	154	291	0.53	0.04837	0.00229	0.16609	0.00802	0.02491	0.00066	117.3	100.1	156.0	6.3	158.6	2.3
-2	3	88	172	0.51	0.05412	0.00334	0.18128	0.01113	0.0243	0.0007	375.6	126.4	169.2	9.0	154.8	2.7
-3	5	176	320	0.55	0.05326	0.00254	0.17499	0.00846	0.02383	0.00064	339.8	96.5	163.7	6.6	151.8	2.3
-4	4	54	119	0.45	0.05206	0.0043	0.17117	0.01393	0.02385	0.00074	288.1	172.2	160.4	11.7	151.9	3.0
-5	4	83	165	0.50	0.04825	0.00292	0.1658	0.01006	0.02492	0.00069	111.6	130.5	155.8	8.2	158.7	2.6
-6	4	72	182	0.40	0.05259	0.0032	0.17791	0.01079	0.02453	0.0007	311.1	126.2	166.3	8.7	156.2	2.6
-7	5	414	447	0.92	0.04813	0.00217	0.15877	0.0073	0.02392	0.00062	105.5	94.7	149.6	5.7	152.4	2.2
-8	6	255	187	1.36	0.04892	0.00222	0.1603	0.00721	0.02377	0.00071	143.8	102.9	151.0	6.3	151.5	4.4
-9	10	208	331	0.63	0.04991	0.00166	0.16655	0.00576	0.02421	0.00067	190.8	75.5	156.4	5.0	154.2	4.2

续表 2

Continued Table 2

测点号	含量($\times10^{-6}$)			Th/U	同位素比值						年龄(Ma)					
	Pb	Th	U		$^{207}Pb/^{206}Pb$	1σ	$^{207}Pb/^{235}U$	1σ	$^{206}Pb/^{238}U$	1σ	$^{207}Pb/^{206}Pb$	1σ	$^{207}Pb/^{235}U$	1σ	$^{206}Pb/^{238}U$	1σ
-10	18	395	607	0.65	0.04811	0.00137	0.15476	0.00478	0.02334	0.00062	104.7	65.8	146.1	4.2	148.7	3.9
-11	10	144	362	0.40	0.04955	0.00177	0.17191	0.00629	0.02517	0.00071	173.7	81.5	161.1	5.5	160.3	4.5
-12	14	204	456	0.45	0.05277	0.00183	0.17994	0.0064	0.02474	0.0007	318.8	77.1	168.0	5.5	157.5	4.4
-13	7	120	247	0.48	0.04900	0.00188	0.16465	0.00643	0.02438	0.00069	148.0	87.4	154.8	5.6	155.2	4.4
-14	13	293	437	0.67	0.04994	0.00152	0.15918	0.00517	0.02312	0.00063	192.3	69.4	150.0	4.5	147.4	4.0
-15	8	143	279	0.51	0.05194	0.00237	0.17474	0.00802	0.02441	0.00071	282.8	101.1	163.5	6.9	155.4	4.5
-16	14	202	537	0.38	0.04959	0.00137	0.15815	0.00482	0.02313	0.00062	176.0	63.3	149.1	4.2	147.4	3.9
-17	10	152	355	0.43	0.05017	0.00157	0.16524	0.00549	0.02389	0.00066	202.8	71.1	155.3	4.8	152.2	4.1
-18	12	248	394	0.63	0.04919	0.00149	0.16042	0.00524	0.02366	0.00065	156.9	69.6	151.1	4.6	150.7	4.1
-19	20	354	683	0.52	0.04932	0.00141	0.17255	0.00539	0.02538	0.00069	163.2	65.6	161.6	4.7	161.6	4.3
-20	14	140	324	0.43	0.05273	0.00184	0.17204	0.00621	0.02367	0.00067	317.2	77.4	161.2	5.4	150.8	4.2
-21	12	715	296	2.42	0.05066	0.00153	0.1772	0.00575	0.02537	0.0007	225.4	68.2	165.6	5.0	161.5	4.4
-22	12	234	355	0.66	0.05044	0.00202	0.16793	0.00675	0.02415	0.00072	215.3	90.2	157.6	5.9	153.8	4.5
-23	6	111	191	0.58	0.04921	0.0017	0.17293	0.00625	0.02549	0.00072	157.9	79.0	162.0	5.4	162.3	4.5
-24	9	94	181	0.52	0.05106	0.00166	0.17342	0.00597	0.02463	0.00069	243.7	73.0	162.4	5.2	156.9	4.3
-25	8	146	262	0.56	0.04901	0.00195	0.17172	0.00692	0.02542	0.00075	148.3	90.6	160.9	6.0	161.8	4.7
-26	10	198	336	0.59	0.04921	0.00129	0.16458	0.0049	0.02426	0.00065	157.8	60.1	154.7	4.3	154.5	4.1
-27	9	129	314	0.41	0.05037	0.00155	0.16891	0.00559	0.02432	0.00068	212.2	69.6	158.5	4.9	154.9	4.3
-28	43	908	1494	0.61	0.05144	0.00219	0.17685	0.0076	0.02494	0.00075	260.6	95.0	165.3	6.6	158.8	4.7
-29	11	171	399	0.43	0.04886	0.00174	0.1609	0.00599	0.02389	0.00069	140.9	81.7	151.5	5.2	152.2	4.4
-30	6	83	197	0.42	0.04969	0.00184	0.16358	0.00628	0.02387	0.0007	180.5	84.1	153.8	5.5	152.1	4.4
-31	10	187	308	0.61	0.05018	0.00157	0.17744	0.006	0.02564	0.00073	203.3	71.1	165.9	5.2	163.2	4.6
-32	13	270	408	0.66	0.04956	0.00149	0.17569	0.0058	0.02571	0.00072	174.2	68.9	164.3	5.0	163.6	4.5
-33	41	894	1251	0.71	0.05006	0.00174	0.17384	0.00637	0.02518	0.00073	197.8	78.8	162.7	5.5	160.3	4.6
-34	9	137	303	0.45	0.05133	0.00218	0.17801	0.00765	0.02515	0.00077	255.7	94.9	166.3	6.6	160.1	4.9
-35	7	124	248	0.50	0.04888	0.0015	0.16256	0.00546	0.02411	0.00068	142.3	70.3	152.9	4.8	153.6	4.3
-36	18	269	602	0.45	0.04924	0.00184	0.16508	0.0064	0.02431	0.00072	159.2	85.2	155.1	5.6	154.8	4.5
-37	9	144	297	0.49	0.04841	0.00132	0.15929	0.00496	0.02386	0.00066	119.2	63.0	150.1	4.3	152.0	4.2

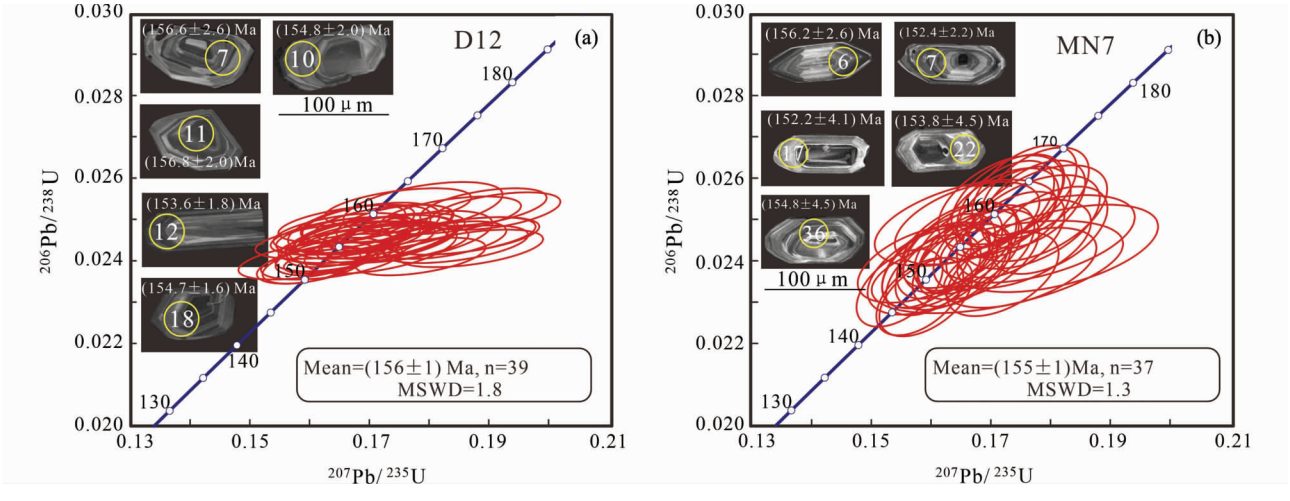

图 3 突泉地区晚侏罗世流纹岩(a)和英云闪长玢岩(b)LA-ICP-MS 锆石 U-Pb 年龄谐和图及部分测定锆石 CL 图像

Fig. 3 LA-ICP-MS zircon U-Pb concordia diagrams for rhyolite (a) and tonalite porphyrites (b) in the Tuquan area, show typical CL images of zircons with U-Pb ages

表 3 突泉地区流纹岩和英云闪长玢岩主量元素(wt%)和微量元素($\times10^{-6}$)分析结果

Table 3 Major (wt%) and trace ($\times10^{-6}$) element compositions of the rhyolites and tonalite porphyrites in the Tuquan area

样品号	D11	D12	D13	D14	MN6	MN7	MN10	MN11	MN12
岩性	流纹岩				英云闪长玢岩				
SiO_2	74.28	72.35	72.52	73.05	69.75	68.23	72.47	72.13	70.62
TiO_2	0.27	0.29	0.37	0.31	0.29	0.30	0.29	0.28	0.29
Al_2O_3	13.70	14.65	14.21	14.18	16.65	18.16	17.40	17.18	17.34
Fe_2O_3	1.76	2.22	1.77	1.90	0.63	0.48	0.39	0.37	0.46
FeO	0.63	0.66	1.19	0.79	1.53	1.19	0.36	0.56	0.78
FeO^T	2.21	2.66	2.79	2.54	2.10	1.62	0.71	0.89	1.21
MnO	0.05	0.05	0.04	0.05	0.06	0.07	0.05	0.04	0.05
MgO	0.44	0.53	0.58	0.51	0.43	0.46	0.25	0.30	0.35
CaO	0.16	0.14	0.16	0.15	0.44	0.33	0.06	0.06	0.15
Na_2O	4.08	4.99	4.09	4.37	4.78	4.76	3.72	4.06	4.31
K_2O	2.67	2.39	3.11	2.71	2.38	1.73	1.76	1.69	1.87
P_2O_5	0.03	0.04	0.05	0.04	0.07	0.05	0.03	0.03	0.04
LOI	1.65	1.60	1.73	1.66	3.02	3.77	3.21	3.03	3.24
Total	99.73	99.91	99.82	99.82	100.02	99.53	100.01	99.74	99.82
$Mg^{\#}$	26.27	26.18	26.95	26.47	26.77	33.58	38.53	37.46	33.75
K_2O+Na_2O	6.75	7.38	7.20	7.08	7.16	6.49	5.48	5.75	6.18
K_2O/Na_2O	0.65	0.48	0.76	0.62	0.50	0.36	0.47	0.42	0.43
La	26.07	22.23	17.02	21.45	13.71	13.77	12.99	7.84	11.77
Ce	57.11	47.50	36.87	46.42	27.77	27.68	26.90	14.71	23.48
Pr	6.79	5.94	4.43	5.63	3.56	3.75	3.30	2.30	3.17
Nd	25.07	22.31	16.62	21.03	13.43	14.30	12.13	8.72	11.94
Sm	4.86	4.43	3.23	4.11	2.57	2.73	2.22	1.69	2.26
Eu	0.80	0.88	0.76	0.81	0.44	0.36	0.24	0.20	0.30
Gd	4.44	4.04	2.77	3.68	2.45	2.54	1.99	1.49	2.07
Tb	0.66	0.66	0.45	0.58	0.36	0.35	0.28	0.22	0.30
Dy	3.73	3.85	2.67	3.37	2.15	1.93	1.62	1.21	1.69
Ho	0.81	0.82	0.56	0.72	0.43	0.35	0.30	0.23	0.32
Er	2.22	2.36	1.76	2.09	1.23	0.94	0.84	0.63	0.88
Tm	0.34	0.38	0.28	0.33	0.19	0.13	0.12	0.09	0.13
Yb	2.13	2.40	1.84	2.11	1.24	0.80	0.70	0.53	0.78
Lu	0.34	0.38	0.30	0.34	0.19	0.12	0.10	0.08	0.12
Rb	84.57	66.36	78.83	76.20	41.01	35.75	37.24	24.89	34.14
Ba	624.2	659.3	664.2	648.9	517.2	136.1	315.1	244.1	271.2
Th	9.49	8.68	6.60	8.16	3.73	3.89	3.54	2.34	3.31
U	3.13	3.42	4.27	3.58	1.12	1.26	1.09	0.89	1.08
Nb	8.50	8.34	7.66	8.16	7.55	8.20	7.73	7.44	7.72
Ta	0.92	0.96	0.78	0.88	0.40	0.42	0.41	0.42	0.41
Pb	13.25	12.41	7.77	10.85	4.84	5.98	3.55	4.11	4.53
Sr	152.4	143.6	154.9	150.2	117.0	87.4	100.0	60.6	88.7
Zr	302.3	323.8	335.8	320.3	283.2	321.9	313.3	313.9	307.7
Hf	9.57	10.15	9.95	9.89	7.57	8.30	8.41	8.28	8.13
Sc	4.87	7.46	4.49	5.46	4.81	4.19	3.33	4.51	4.17
V	18.59	23.37	28.34	23.09	2.07	2.35	2.88	2.23	2.36
Cr	7.68	6.38	8.91	7.58	8.88	12.49	9.51	9.20	9.93
Co	1.80	2.45	3.13	2.40	1.91	1.59	1.73	0.90	1.47
Ni	3.23	3.05	2.77	3.01	2.19	2.77	4.36	1.70	2.59
Ga	18.68	20.86	20.49	19.99	18.33	17.39	16.05	17.31	17.25
Y	19.44	19.75	13.36	17.25	12.26	10.57	8.22	5.29	8.67
Cs	3.44	3.75	3.72	3.63	1.26	1.00	0.94	0.79	0.98
δEu	0.52	0.62	0.76	0.63	0.53	0.42	0.34	0.39	0.41
$(La/Yb)_N$	8.77	6.64	6.62	7.28	7.93	12.29	13.39	10.57	10.83

续表 3

Continued Table 3

样品号	D11	D12	D13	D14	MN6	MN7	MN10	MN11	MN12
岩性	流纹岩				英云闪长玢岩				
∑REE	135.4	118.2	89.56	112.7	69.71	69.75	63.71	39.92	59.30
A/CNK	1.39	1.32	1.36	1.36	1.48	1.76	2.13	1.99	1.82
A/NK	1.42	1.35	1.40	1.39	1.59	1.87	2.16	2.01	1.90
C	3.93	3.77	4.00	3.90	5.75	8.33	9.65	8.93	8.02
Q	39.90	33.17	36.18	36.31	31.54	33.45	45.14	42.83	37.79
Ab	35.26	42.97	35.30	37.68	41.72	42.08	32.53	35.53	37.74
Or	16.11	14.38	18.73	16.31	14.50	10.68	10.75	10.33	11.45
An	0.64	0.44	0.52	0.53	1.77	1.36	0.10	0.10	0.39
Hy	1.69	2.82	2.09	2.15	3.08	2.68	0.64	1.11	1.56
Il	0.52	0.56	0.71	0.59	0.56	0.59	0.56	0.54	0.56
Mt	1.86	1.80	2.36	1.99	0.94	0.72	0.52	0.55	0.66
Ap	0.06	0.08	0.10	0.08	0.16	0.12	0.07	0.07	0.10

注：$FeO^T = FeO + 0.8998 \times Fe_2O_3$；$Mg^{\#} = 100 \times MgO/(MgO + FeO^T)$；$\delta Eu = Eu_N/(Sm_N \times Gd_N)^{0.5}$；$A/CNK = Al_2O_3/(CaO + Na_2O + K_2O)$；$A/NK = Al_2O_3/(Na_2O + K_2O)$；CIPW 为标准化矿物含量；C 为刚玉；Q 为石英；Ab 为钠长石；Or 为正长石；An 为钙长石；Hy 为紫苏辉石；Il 为钛铁矿；Mt 为磁铁矿；Ap 为磷灰石

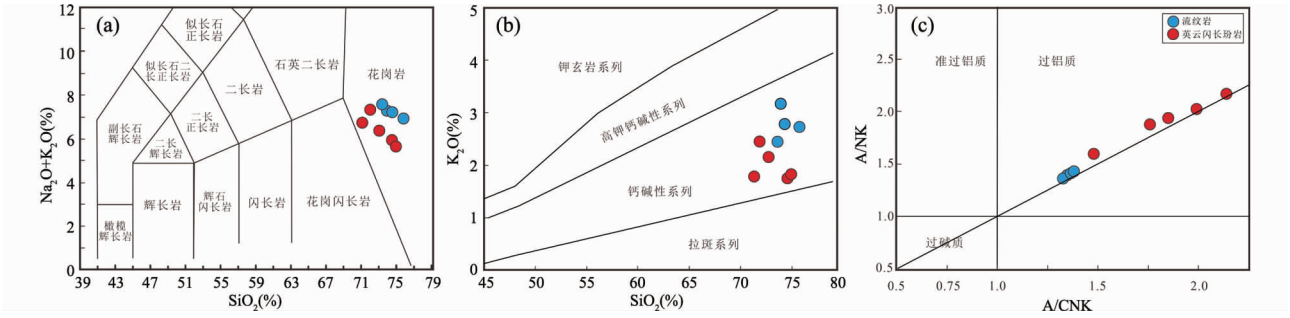

图 4　突泉地区流纹岩和英云闪长玢岩 SiO_2-($Na_2O + K_2O$)图解(a,据 Middlemost, 1994)、SiO_2-K_2O 图解(b,据 Peccerillo and Taylor, 1976)和 A/CNK-A/NK 图解(c,据 Maniar and Piccoli, 1989)

Fig. 4　SiO_2 vs. ($Na_2O + K_2O$) classification diagram (a, after Middlemost, 1994), SiO_2 vs. K_2O diagram (b, after Peccerillo and Taylor, 1976) and A/CNK vs. A/NK (c, after Maniar and Piccoli, 1989) of the rhyolites and tonalite porphyrites in the Tuquan area

岩形成于晚侏罗世(图 3b、表 2)。

3.2　地球化学特征

突泉地区流纹岩和英云闪长玢岩主量元素和微量元素分析结果见表 3。

3.2.1　主量元素

流纹岩的 SiO_2 含量为 72.35% ~ 74.28%；Al_2O_3 含量为 13.70% ~ 14.65%；Na_2O 含量为 4.08% ~ 4.99%；K_2O 含量为 2.39% ~ 3.11%；MgO 含量为 0.44% ~ 0.58%；全碱($Na_2O + K_2O$)含量为 6.74% ~ 7.38%；K_2O/Na_2O 值为 0.48 ~ 0.76。

英云闪长玢岩的 SiO_2 含量为 68.23% ~ 72.47%；Al_2O_3 含量为 16.65% ~ 18.16%；Na_2O 含量为 3.72% ~ 4.78%；K_2O 含量为 1.69% ~ 2.38%；MgO 含量为 0.25% ~ 0.46%；全碱($Na_2O + K_2O$)含量为 5.48% ~ 7.16%；K_2O/Na_2O 值为 0.36 ~ 0.50。

在 TAS 分类图解中，两种岩石样品均投点在花岗岩区域内(图 4a)，在 SiO_2-K_2O 图解中(图 4b)，样品投点在钙碱性系列。在 A/NK-A/CNK 图解中(图 4c)，两种岩石投点在过铝质区域。其中流纹岩铝饱和指数 A/CNK 值为 1.32 ~ 1.39，平均值为 1.36，英云闪长玢岩铝饱和指数 A/CNK 值为 1.48 ~ 2.13，平均值为 1.84。

3.2.2　微量元素

流纹岩稀土元素总量(∑REE)为 89.56×10^{-6} ~ 135.4×10^{-6}，高于英云闪长玢岩稀土元素总量(∑REE)39.92×10^{-6} ~ 69.75×10^{-6}。流纹岩轻重稀土元素比值(LREE/HREE)为 6.96 ~ 8.23，$(La/Yb)_N$ 值为 6.62 ~ 8.77，δEu 值为 0.52 ~ 0.76，英云闪长玢岩轻重稀土元素比值(LREE/HREE)

表 4 突泉地区及邻区晚侏罗世岩浆岩锆石 U-Pb 测年及构造亲缘性和应力归属

Table 4 Zircon U-Pb dating of Late Jurassic magmatic rocks in Tuquan area and adjacent areas and their structural affinity and stress attribution

位置	岩性	测年数据(Ma)	构造亲缘性	应力归属	资料来源
大兴安岭北段上黑龙江盆地	花岗闪长岩	晚侏罗世	陆-陆碰撞	蒙古-鄂霍茨克洋闭合	武广等, 2008
大兴安岭南段甘珠而庙	二长花岗岩	154 ± 1	陆-陆碰撞	蒙古-鄂霍茨克洋闭合	杨奇荻等, 2014
额尔古纳	正长花岗岩	150.0 ± 2.0	陆-陆碰撞	蒙古-鄂霍茨克洋闭合	Tang *et al.*, 2015
大兴安岭南段扎鲁特盆地坤都	流纹岩	151.2 ± 1.2	俯冲岛弧	蒙古-鄂霍茨克洋俯冲	张超等, 2018
大兴安岭北段伊勒呼里山	二长花岗岩	158.1 ± 0.7	陆-陆碰撞	蒙古-鄂霍茨克洋闭合	尹志刚等, 2018
兴安地块东北部	花岗闪长岩	154.1 ± 1.1	陆-陆碰撞	蒙古-鄂霍茨克洋闭合	赵院冬等, 2018
大兴安岭南部	英安岩	158 ± 1	陆-陆碰撞	蒙古-鄂霍茨克洋闭合	Liu *et al.*, 2018
大兴安岭中段五岔沟	流纹岩	154 ± 1	陆-陆碰撞后伸展	蒙古-鄂霍茨克洋闭合	Ji *et al.*, 2018
大兴安岭南段东乌旗东部	流纹岩	150.9 ± 4.2	俯冲岛弧	蒙古-鄂霍茨克洋俯冲	尹志刚等, 2019
海拉尔盆地	流纹岩	154 ± 2	陆-陆碰撞	蒙古-鄂霍茨克洋闭合	Ji *et al.*, 2019
大兴安岭北段黑河地区	二长花岗岩	153.5 ± 0.56	俯冲岛弧	蒙古-鄂霍茨克洋俯冲	贺国奇等, 2020
大兴安岭中部柴河地区	二长花岗岩	152.0 ± 1.0	陆-陆碰撞	蒙古-鄂霍茨克洋闭合	施璐等, 2020
大兴安岭南段巴林左旗-扎鲁特旗地区	流纹岩	154 ± 1	陆-陆碰撞	蒙古-鄂霍茨克洋闭合	Zhang *et al.*, 2020
松辽盆地西部突泉地区	煌斑岩	156.0 ± 2.3	俯冲岛弧	蒙古-鄂霍茨克洋俯冲	Yu *et al.*, 2022

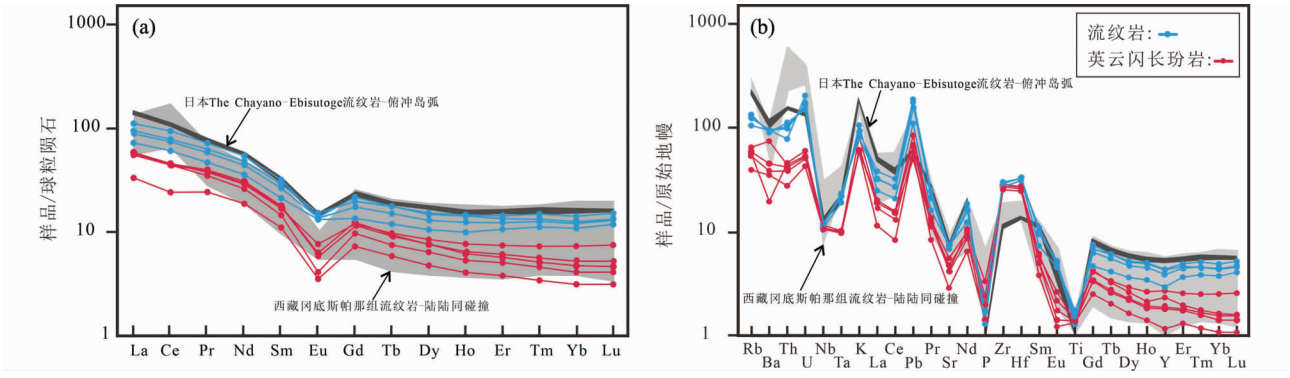

图 5 突泉地区流纹岩和英云闪长玢岩球粒陨石标准化稀土元素配分图(a)和原始地幔标准化微量元素蛛网图(b)(标准化数值据 Sun and McDonough, 1989)

数据来源:西藏新生代冈底斯帕那组流纹岩-陆陆同碰撞环境(Mo *et al.*, 2007);日本新生代 The Chayanao-Ebisutoge 流纹岩-俯冲岛弧环境(Kimura and Nagahashi, 2007)

Fig. 5 chondrite-normalized REE patterns (a) and primitive mantle-normalized spider diagram (b) of the rhyolites and tonalite porphyrites in the Tuquan area (normalization values after Sun and McDonough, 1989)

Data sources: the Gangdese rhyolite in southern Tibet (Mo *et al.*, 2007), the Chayanao-Ebisutoge rhyolite in Japan (Kimura and Nagahashi, 2007)

为 7.47 ~ 9.71,$(La/Yb)_N$ 值为 7.93 ~ 13.39,δEu 值为 0.34 ~ 0.53,均呈现 Eu 负异常,表现出轻稀土元素相对富集,重稀土元素亏损的特征(图 5a);在原始地幔标准化微量元素蛛网图中(图 5b),流纹岩和英云闪长玢岩呈现出富集 Rb、Ba、K 等大离子亲石元素,亏损 Nb、Ta、Ti 等高场强元素特征。流纹岩和英云闪长玢岩的稀土元素配分模式和微量元素特征均与岛弧和同碰撞流纹岩的特征相似(Mo *et al.*, 2007; Kimura and Nagahashi, 2007)。

4 讨论

4.1 流纹岩和英云闪长玢岩的形成时代

松辽盆地西缘突泉地区的流纹岩和英云闪长玢岩锆石 CL 图像(图 3)可以清晰看出锆石具有典型的岩浆振荡生长环带,而且具有较高的 Th/U 比值(0.20 ~ 2.42),说明其为岩浆锆石(Hoskin and Schaltegger, 2003)。锆石 U-Pb 测年分析点多位于锆石的环带部位,数据投点在 U-Pb 谐和线上,表明这些测年结果代表锆石的结晶年龄,进而可以代表样品形成时代。

流纹岩单颗粒锆石的 $^{206}Pb/^{238}U$ 年龄值介于 152.1 ± 1.6Ma ~ 161.0 ± 1.8Ma 之间,加权平均年龄为 156 ± 1Ma (MSWD = 1.8),英云闪长玢岩单颗粒锆石的 $^{206}Pb/^{238}U$ 年龄值介于 147.4 ± 3.9Ma ~ 163.6 ± 4.5Ma 之间,加权平均年龄为 155 ± 1Ma(MSWD = 1.3),表明突泉地区流纹岩和英云闪长玢岩形成时代为晚侏罗世,且流纹岩结晶年龄大于英云闪

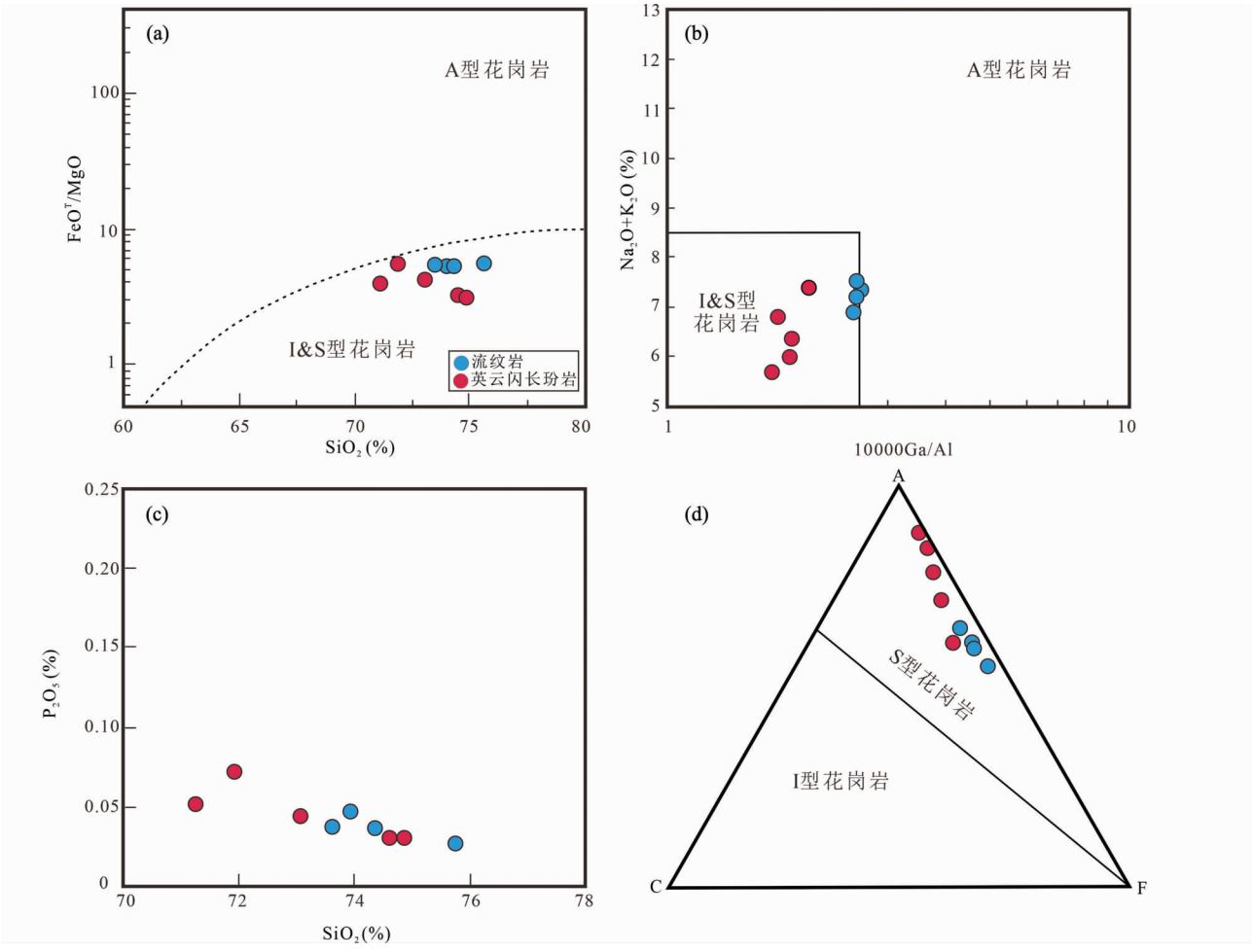

图 6　突泉地区流纹岩和英云闪长玢岩岩石成因类型判别图解

(a) FeO^T/MgO-SiO_2 图解(据 Eby, 1990)；(b) Na_2O+K_2O-10000Ga/Al 图解(据 Whalen *et al.*, 1987)；(c) P_2O_5-SiO_2 图解；(d) A(Al-Na-K)-C(Ca)-F($Mg+Fe^{2+}$)图解(据 White and Chappell, 1977)

Fig. 6　Rock type discrimination diagrams for the rhyolites and tonalite porphyrites in the Tuquan area

(a) FeO^T/MgO vs. SiO_2 (after Eby, 1990); (b) Na_2O+K_2O vs. 10000Ga/Al (after Whalen *et al.*, 1987); (c) P_2O_5 vs. SiO_2; (d) A (Al-Na-K) vs. C (Ca) vs. F ($Mg+Fe^{2+}$) (after White and Chappell, 1977)

长玢岩结晶年龄。

松辽盆地西缘流纹岩和英云闪长玢岩形成于晚侏罗世，这与研究区内正长花岗岩和花岗闪长岩岩体(150～160Ma；Wu *et al.*, 2011；Tang *et al.*, 2015)、大兴安岭中南段甘珠尔庙地区黑云母正长花岗岩岩体(154Ma；杨奇荻等, 2014)、兴安地块黑花山埃达克质花岗岩岩体(158～154Ma；赵院冬等, 2018)、大兴安岭北端的龙沟河、二十一站等岩体(武广等, 2008)和额尔古纳地块、兴安地块酸性火山岩(148～160Ma；Zhang *et al.*, 2010；Ji *et al.*, 2019；Zhang *et al.*, 2020)的形成时代一致，具有相同的岩浆活动时期和构造背景(表 4)。

4.2　流纹岩和英云闪长玢岩成因类型

晚侏罗世流纹岩和英云闪长玢岩矿物组成主要为石英、钾长石、斜长石和绢云母，其中绢云母的成分基本上和白云母相同 $K\{Al_2[AlSi_3O_{10}](OH)_2\}$，为富铝矿物，不含有 A 型花岗岩中经常出现的碱性铁镁质暗色矿物(钠闪石等)，也不含 I 型花岗岩特征矿物角闪石。流纹岩和英云闪长玢的 CIPW 标准矿物计算结果显示含刚玉分子(3.77%～9.65%)(表 3)，与过铝质花岗岩特征相似(Chappell and White, 2001)。流纹岩和英云闪长玢岩富 SiO_2(68.23%～74.28%)、低 $MgO+FeO^T$(0.96%～3.37%)，铝饱和指数 A/CNK(1.32～2.13)大于 1.1，为强过铝质花岗岩(Sylvester, 1998)。流纹岩和英云闪长玢岩的 FeO^T/MgO 比值较低(2.84～5.02)，与 A 型花岗岩类明显富铁的特征不相同($FeO^T/MgO>10$, Whalen *et al.*, 1987)。在 SiO_2-FeO^T/MgO 关系图中(图 6a)，样品投点在 I 型、S 型花岗岩区内。流纹岩和英云闪长玢岩的 $10^4\times Ga/Al$ 为 1.69～2.67，在以 $10^4\times$

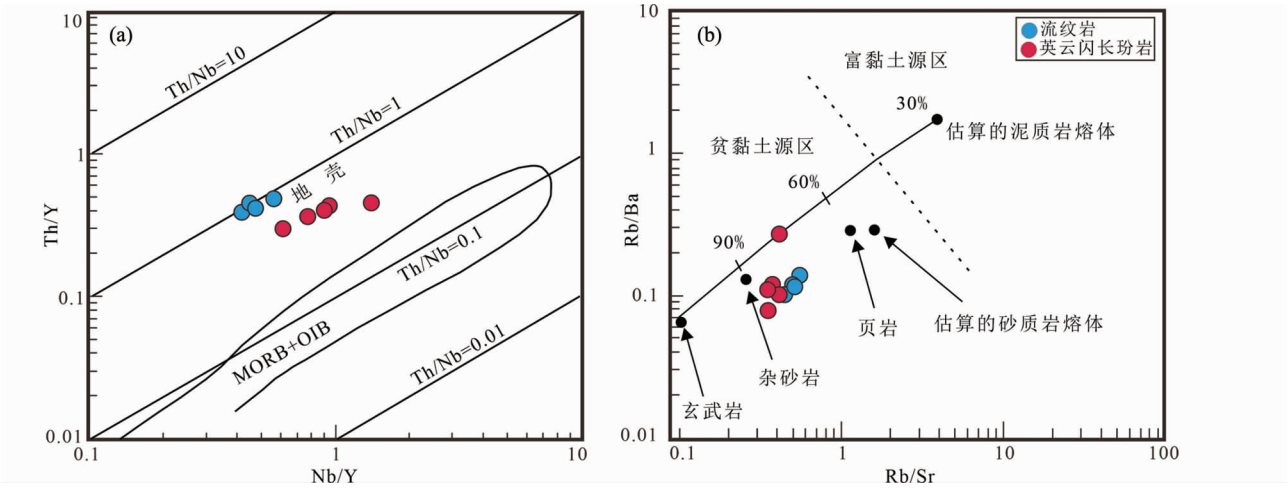

图 7 突泉地区流纹岩和英云闪长玢岩成因判别 Th/Y-Nb/Y 图解(a,据 Boztuğ *et al.*, 2007)和 Rb/Ba-Rb/Sr 图解(b 据 Sylvester, 1998)

Fig. 7 Petrogenetic discrimination diagrams of Th/Y vs. Nb/Y (a, after Boztuğ *et al.*, 2007) and Rb/Ba vs. Rb/Sr (b, after Sylvester, 1998) for the rhyolites and tonalite porphyrites in the Tuquan area

Ga/Al 比值为基础的判别图解中(图 6b),样品大部分投点于 I 型、S 型花岗岩区域内。岩石学实验表明,在过铝质岩浆中,P_2O_5 含量稳定,不随 SiO_2 含量的变化而变化,这种地球化学特征可用于区分 I 型和 S 型花岗岩(Watson and Capobianco, 1981),流纹岩和英云闪长玢岩样品的 P_2O_5 变化较小(0.03% ~ 0.07%),在 SiO_2-P_2O_5 图解中(图 6c),P_2O_5 含量随着 SiO_2 含量增加基本保持稳定,与 S 型花岗岩的演化趋势较一致。此外,在 ACF 图解中(图 6d),流纹岩和英云闪长玢岩样品均投点在 S 型花岗岩范围。上述结果综合表明流纹岩和英云闪长玢岩具有过铝质 S 型花岗岩特征。

4.3 流纹岩和英云闪长玢岩岩浆源区性质

晚侏罗世流纹岩和英云闪长玢岩为长英质酸性火成岩,具有较高的 SiO_2(68.23% ~ 74.28%)含量,较低的 MgO(0.25% ~ 0.58%)、Cr(6.38×10^{-6} ~ 12.49×10^{-6})、Co(0.90×10^{-6} ~ 3.13×10^{-6})、Ni(1.70×10^{-6} ~ 4.36×10^{-6})含量,与基性岩地球化学特征不同,同时研究区缺少与之同生的大规模铁镁质火山岩,表明流纹岩和英云闪长玢岩起源于幔源岩浆分异的可能性较小。

流纹岩和英云闪长玢岩的 Nb/U 比值(1.79 ~ 8.36)和 Rb/Sr 比值(0.35 ~ 0.55)与大陆地壳平均值相近(Nb/U = 6.2; Rudnick and Fountain, 1995; Rb/Sr = 0.35; Hofmann *et al.*, 1986),而明显不同于地幔平均值(Nb/U = 47 ± 10; Rudnick and Fountain, 1995; Rb/Sr = 0.034; Hofmann *et al.*, 1986)。在 Nb/Y-Th/Y 图解中(图 7a),流纹岩和英云闪长玢岩投点在壳源附近,暗示其源岩来自地壳物质的部分熔融。

过铝质 S 型花岗岩是变质沉积岩部分熔融的产物(Sylvester, 1998)。变质沉积岩既包含"成熟度"较高的富黏土泥岩(Searle *et al.*, 1997),又包含"成熟度"相对较低的贫黏土杂砂岩(White and Chappell, 1988)。一般认为源区为富黏土泥岩的过铝质熔体具有较高的 Rb/Sr 和 Rb/Ba 值,而源区为贫黏土杂砂岩的过铝质熔体具有较低的 Rb/Sr 和 Rb/Ba 值。流纹岩和英云闪长玢岩样品的 Rb/Sr 值为 0.35 ~ 0.55,Rb/Ba 值为 0.08 ~ 0.26。在 Rb/Sr-Rb/Ba 图解中(图 7b),流纹岩和英云闪长玢岩样品均投点在贫黏土变质杂砂岩部分熔融区附近,表明流纹岩和英云闪长玢岩为贫黏土源区杂砂岩部分熔融,流纹岩起源于熔融程度为 75% ~ 80% 的杂砂岩,英云闪长玢岩起源于熔融程度为 70% ~ 90% 的杂砂岩。

在部分熔融过程中,含铝矿物随着温度的升高,铝含量基本不变,而含钛矿物随着温度的升高,钛含量也升高。因此部分熔融的温度越高,Al_2O_3/TiO_2 比值越小(Patiño Douce and Johnston, 1991)。流纹岩和英云闪长玢岩 Al_2O_3/TiO_2 比值为 38.41 ~ 61.36,表明其部分熔融温度较低,这与锆饱和温度估算的流纹岩和英云闪长玢岩初始源区岩浆的温度 T_{Zr}(850 ~ 876℃)和(837 ~ 849℃)一致(Miller *et al.*, 2003)。综合推断流纹岩和英云闪长玢岩岩浆形成温度小于 875℃,低于 A 型花岗岩岩浆形成温度(900℃)。

4.4 地球动力学背景

研究区流纹岩和英云闪长玢岩主量元素地球化学分析显示 Al_2O_3 含量较高为 13.70% ~ 18.16%,TiO_2 含量较低为 0.27% ~ 0.37%,与俯冲岛弧和同碰撞背景下的岩浆岩地球化学特征相似(Crawford *et al.*, 1987; Kimura and Nagahashi, 2007; Mo *et al.*, 2007)。微量元素地球化学分析显示,流纹岩和英云闪长玢岩富集 Rb、Ba、K 等大离子亲石元素,亏损 Nb、Ta、P、Ti 等高场强元素。具有较低的 Y(5.29×10^{-6} ~ 19.75×10^{-6})、Nb(7.44×10^{-6} ~ 8.50×10^{-6})、Sr(60.6 ×

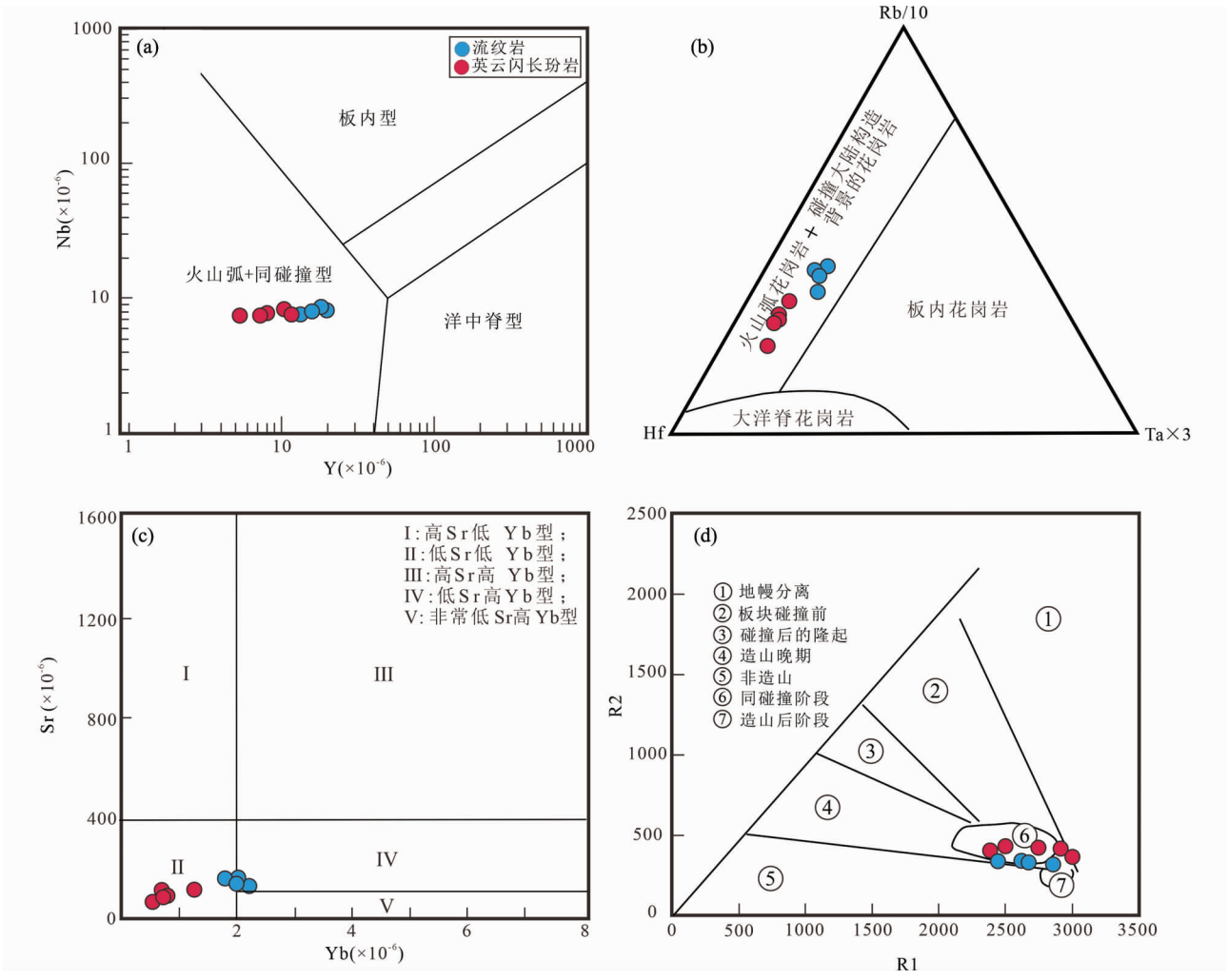

图 8　突泉地区流纹岩和英云闪长玢岩构造环境判别图解

(a) Nb-Y 图解(据 Pearce *et al.*, 1984)；(b) Rb/10-Hf-Ta×3 图解(据 Harris *et al.*, 1986)；(c) Sr-Yb 图解(据张旗等,2008)；(d) R1-R2 图解(据 Batchelor and Bowden, 1985)，R1 = 4Si-11(Na + K)-2(Fe + Ti))，R2 = 6Ca + 2Mg + Al

Fig. 8　Tectonic discrimination diagrams for the rhyolites and tonalite porphyrites in the Tuquan area

(a) Nb vs. Y (after Pearce *et al.*, 1984); (b) Rb/10 vs. Hf vs. Ta×3 (after Harris *et al.*, 1986); (c) Sr vs. Yb (after Zhang *et al.*, 2008); (d) R1 vs. R2 (after Batchelor and Bowden, 1985)

10^{-6} ~ 154.9 × 10^{-6})和 Yb(0.53 × 10^{-6} ~ 2.40 × 10^{-6})含量，与岛弧花岗岩类似(Pearce, 1983)。从酸性岩稀土和微量元素亲缘关系看(图 5)，研究区流纹岩(156Ma)与日本新生代 The Chayanao-Ebisutoge 俯冲岛弧环境流纹岩更接近(Kimura and Nagahashi, 2007)，而英云闪长玢岩表现出与西藏冈底斯帕那组新生代陆-陆同碰撞环境流纹岩相似的稀土和微量元素分配模式(Mo *et al.*, 2007)。

Pearce *et al.* (1984)将花岗岩侵入环境分为洋中脊型、板内型、火山弧型和同碰撞型，并建立了 Y-Nb 元素判别图解。在 Y-Nb 图解(图 8a)中流纹岩和英云闪长玢岩投点在火山弧和同碰撞型花岗岩区域内，流纹岩具有相对高的 Y 值。Harris *et al.* (1986)利用 Rb-Hf-Ta 三元图解按照构造演化阶段将酸性岩浆岩划分为碰撞前钙碱性(火山弧)花岗岩、同碰撞过铝质花岗岩、碰撞晚期钙碱性花岗岩和碰撞后花岗岩。在 Rb/10-Hf-Ta×3 图解(图 8b)中，流纹岩和英云闪长玢岩投点在火山弧和碰撞型花岗岩区域内，流纹岩具有相对高的 Rb 和 Ta 值，表明研究区过铝质流纹岩和英云闪长玢岩主要与火山弧花岗岩和同碰撞花岗岩特征相似，可能形成于碰撞前到同碰撞阶段。张旗等(2008)认为中酸性岩浆岩 Sr 和 Yb 的含量与岩浆形成深度有关，是识别与判别岩浆源区成因和性质的有效标志，按照 Sr = 400 × 10^{-6} 和 Yb = 2 × 10^{-6} 的标志将花岗岩划分为 5 类，按照分类，突泉地区过铝质流纹岩属于低 Sr 高 Yb 型，形成于低压环境；英云闪长玢岩属于低 Sr、低 Yb 型，形成于中压环境(图 8c)。根据 Sr 和 Yb 数值变化，突泉地区地壳具有从正常地壳(Sr < 400 × 10^{-6}，Yb > 2 × 10^{-6})向增厚地壳(Sr < 100 × 10^{-6}，Yb < 2 × 10^{-6})演化趋势，即处于地壳加厚阶段(张旗等, 2011)。Batchelor and Bowden (1985)认为花岗岩在 R_1-R_2 岩石分类图解中具

有造山旋回演化特征,在 R_1-R_2 图解中(图 8d),流纹岩构造环境在非造山阶段和同碰撞阶段,英云闪长玢岩构造环境为同碰撞阶段。暗示研究区过铝质岩石的形成可能经历了碰撞前到同碰撞阶段。

过铝质花岗岩具有较高的 SiO_2 含量和铝饱和指数(A/CNK),是杂砂岩或泥质岩部分熔融的产物,形成于陆-陆碰撞环境(Chappell and White, 2001)。Sylvester (1998)认为强过铝质花岗的形成环境可分为同碰撞型和后碰撞型,同碰撞型过铝质花岗岩形成于碰撞早期的地壳加厚阶段,部分熔融的热源为 K、Th、U 等元素的放射性衰变产生的热量,熔融温度一般小于 875℃;后碰撞型过铝质花岗岩形成于地壳加厚之后,部分熔融的热源来自软流圈上涌,熔融温度一般大于 875℃。通过锆饱和温度估算的流纹岩和英云闪长玢岩初始源区岩浆的温度为 850 ~ 876℃和 837 ~ 849℃(Miller *et al.*, 2003),说明其岩浆形成温度小于 875℃,这与阿尔卑斯造山带和喜马拉雅造山带的过铝质花岗岩相似,其形成于陆-陆碰撞过程中地壳加厚阶段(Schärer *et al.*, 1986; von Blanckenburg, 1992)。

流纹岩和英云闪长玢岩重稀土元素含量较低,暗示源区具有石榴子石的残留,结合其过铝质特征,表明它们是加厚陆壳物质部分熔融的产物(Pearce *et al.*, 1990; Harris *et al.*, 1986; Barbarin, 1999)。根据 Profeta *et al.* (2015)归纳的岩浆岩 La/Yb 值与地壳厚度的回归关系式 $H = 21.277\ln(1.0204(La/Yb)_N)$,流纹岩形成时地壳厚度约为 40 ~ 46km,英云闪长玢岩形成时地壳厚度约为 44 ~ 55km,表明地壳处于加厚过程。

大兴安岭地区近年来报道的同期火成岩显示加厚地壳岩浆源区特征(李宇等, 2015; 赵院冬等, 2018; Zhang *et al.*, 2020; Yu *et al.*, 2022),这种加厚地壳预示了同碰撞作用的发生。突泉地区发育中-晚侏罗世前陆盆地(于太极, 2023)、大兴安岭北部漠河地区发育中-晚侏罗世前陆盆地(Tang *et al.*, 2016; Chen *et al.*, 2022),表明在晚侏罗世中国东北地区存在汇聚陆缘边界构造挤压事件,是导致地壳加厚的原因。

结合全球典型的洋壳俯冲岛弧和陆-陆碰撞背景酸性岩地球化学特征和研究区同时期酸性岩特征及区域构造背景,研究区流纹岩和英云闪长玢岩的形成,表明该时期地壳正处于加厚过程,其构造背景为洋壳俯冲到陆-陆碰撞转换阶段。

蒙古-鄂霍茨克缝合带位于研究区西北约 500km,该缝合带西起蒙古中部的杭爱山脉,东至鄂霍茨克的乌达海湾,宽 200 ~ 300km,长度大于 3000km,是蒙古-鄂霍茨克洋闭合的产物。蒙古-鄂霍茨克大洋板块既存在北向俯冲作用(Zorin, 1999; Parfenov *et al.*, 2003; Bussien *et al.*, 2011; Donskaya *et al.*, 2013),也存在南向俯冲作用(Tomurtogoo *et al.*, 2005; Sun *et al.*, 2013; 李宇等, 2015)。蒙古-鄂霍茨克洋自西向东呈剪刀式闭合(Metelkin *et al.*, 2007),最终导致西伯利亚克拉通和蒙古-华北板块碰撞、拼接(赵越等, 1994)。前人的研究表明,东北地区额尔古纳地块、兴安地块中生代岩浆作用与蒙古-鄂霍茨克构造体系密切相关(Meng, 2003; Wang *et al.*, 2006, 2015; Zhang *et al.*, 2010; Wu *et al.*, 2011; Xu *et al.*, 2013; Ouyang *et al.*, 2015; Li *et al.*, 2017; Tang *et al.*, 2019)。松辽盆地西缘突泉地区流纹岩和英云闪长玢岩的成因和形成背景,以及突泉地区晚侏罗世煌斑岩(156.0 ± 2.3Ma;Yu *et al.*, 2022)的起源深度,表明研究区晚侏罗世岩石圈处于增厚阶段,这与蒙古-鄂霍茨克洋闭合后,西伯利亚克拉通与额尔古纳-兴安-松辽地块陆-陆碰撞的动力学背景一致(Zorin, 1999; Oxman, 2003; Metelkin *et al.*, 2010)。晚侏罗世时期沿蒙古-鄂霍茨克缝合带附近发生的褶皱变形、构造不整合和沉积间断等挤压事件,也被认为与蒙古-鄂霍茨克洋闭合以及陆-陆碰撞有关(Li *et al.*, 1999; Tang *et al.*, 2015; Yang *et al.*, 2015)。

也有学者认为东北地区晚中生代岩浆活动与古太平洋板块俯冲角度和速度变化有关(Wu *et al.*, 2002; Zhang *et al.*, 2010, 2011; Ji *et al.*, 2021; Liu *et al.*, 2022)。普遍认为佳木斯地块和松辽地块东部早侏罗世到中侏罗世(194 ~ 174Ma)发育的火成岩与古太平洋板块向西俯冲有关(Guo *et al.*, 2015; Huang *et al.*, 2021)。晚侏罗世到早白垩世早期(173 ~ 133Ma),佳木斯地块和松辽地块存在明显的岩浆活动间歇期(Ji *et al.*, 2019),这表明古太平洋板块俯冲和与俯冲相关的岩浆活动在这一时期逐渐减弱。而在额尔古纳地块和兴安地块晚侏罗世到早白垩世早期(164 ~ 132Ma),岩浆活动频繁,火成岩广泛发育(Zhang *et al.*, 2010; Ji *et al.*, 2021),本文研究的松辽盆地西缘突泉地区晚侏罗世流纹岩和英云闪长玢岩与额尔古纳地块和兴安地块的岩浆活动为同期(表 4),形成于俯冲岛弧和陆-陆碰撞环境,该期岩浆活动同时具有自北向南时代变新的迁移趋势,被认为是与蒙古-鄂霍茨克洋的闭合有关(Zhang *et al.*, 2008, 2010; Ouyang *et al.*, 2015; Li *et al.*, 2017)。在中侏罗世晚期到早白垩世早期,古太平洋板块对欧亚大陆俯冲作用存在间断(Xu *et al.*, 2013; Wang *et al.*, 2019)和俯冲方向的改变(Maruyama *et al.*, 1997),而东北地区中-晚侏罗世到早白垩世早期存在区域不整合和沉积间断,因此蒙古-鄂霍茨克洋的闭合以及陆-陆碰撞解释该时期区域性挤压作用和岩浆活动更为合适(Metelkin *et al.*, 2010; Xu *et al.*, 2013; Yang *et al.*, 2015; 于太极, 2023)。

综上所述,本文认为蒙古-鄂霍茨克构造体系的影响范围到达了松辽盆地西缘突泉地区,研究区晚侏罗世流纹岩和英云闪长玢岩的岩浆活动是蒙古-鄂霍茨克洋洋壳俯冲到陆-陆碰撞的地质响应,松辽盆地西缘及邻区在钦莫利阶(156 ± 1Ma ~ 155 ± 1Ma)处于蒙古-鄂霍茨克洋闭合到陆-陆碰撞转换时期,156 ± 1Ma 时蒙古-鄂霍茨克洋南向俯冲,引发流纹岩岩浆活动;155 ± 1Ma 时西伯利亚板块与额尔古纳-兴安-松辽地块发生陆-陆碰撞,加厚下地壳部分熔融形成英云闪长玢岩岩浆(图 9)。

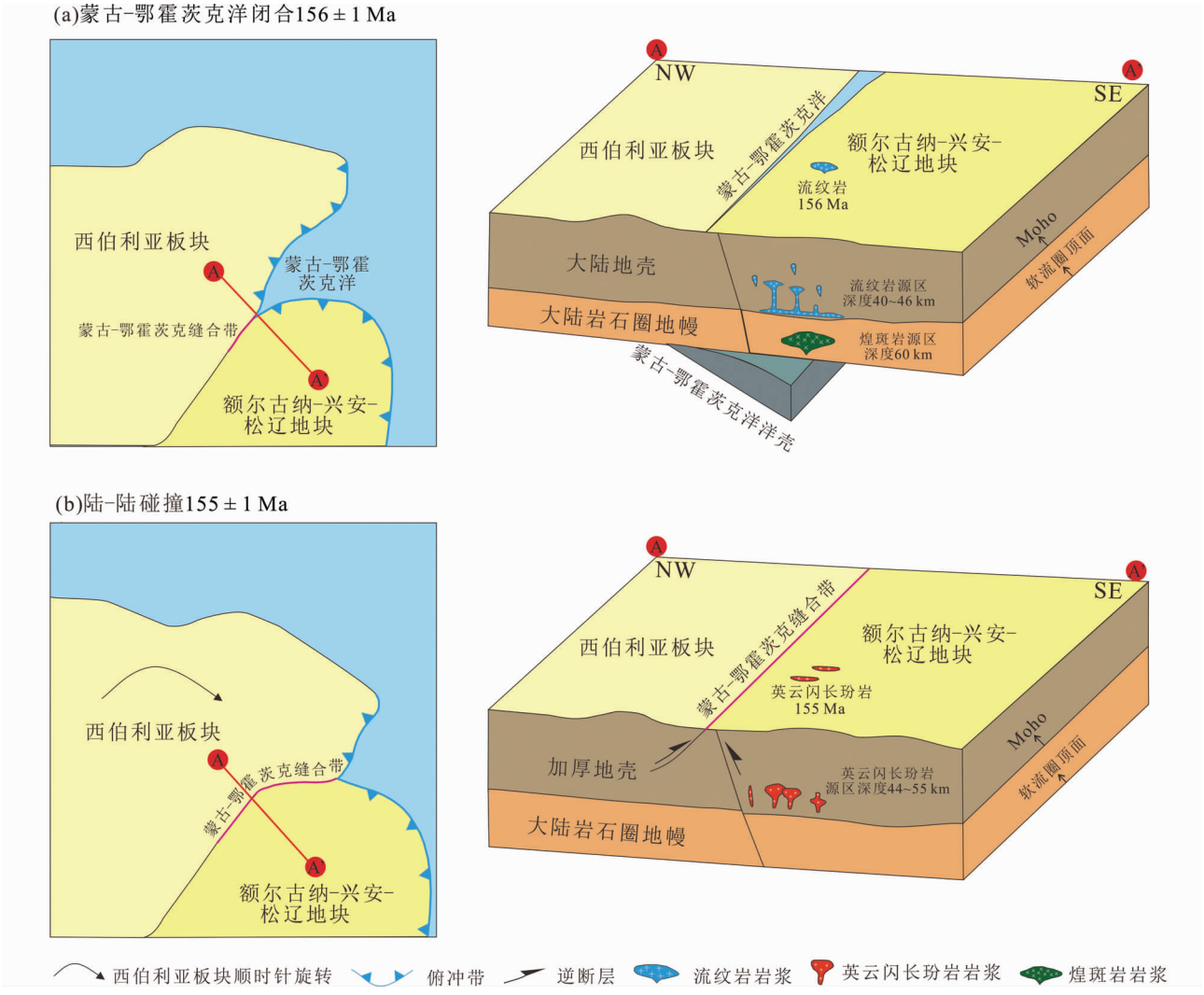

图 9　蒙古-鄂霍茨克洋晚侏罗世地球动力学演化示意图

(a)156±1Ma 蒙古-鄂霍茨克洋南向俯冲,引发流纹岩岩浆活动;(b)155±1Ma 蒙古-鄂霍茨克洋闭合后,西伯利亚板块与额尔古纳-兴安-松辽地块发生陆-陆碰撞,加厚下地壳部分熔融形成英云闪长玢岩岩浆. 西伯利亚板块、额尔古纳-兴安-松辽地块和蒙古-鄂霍茨克洋相对位置及俯冲带和逆断层据 Zorin (1999);西伯利亚板块顺时针旋转据 Metelkin *et al.* (2007);蒙古-鄂霍茨克洋洋壳俯冲据 Ouyang *et al.* (2015);煌斑岩岩浆活动据 Yu *et al.* (2022)

Fig. 9　The cartoon illustrations showing the geodynamic processes for the Mongol-Okhotsk Ocean during the Late Jurassic

(a) the southeastward subduction of the Mongol-Okhotsk Ocean led to rhyolitic magmatic activity at 156±1Ma; (b) the study area at 155±1Ma was at the stage of continental collision and crust thickening after ocean closure, the derivation of tonalite porphyrites magmas from the partial melting of the thickened lower crust. The relative positions of the Siberian Plate, Erguna-Xing'an-Songliao Block, Mongol-Okhotsk Ocean, subduction zones and reverse fault after Zorin (1999); The Siberian plate rotates clockwise after Metelkin *et al.* (2007); The southeastward subduction of the Mongol-Okhotsk Ocean after Ouyang *et al.* (2015); The lamprophyre magmatic activity after Yu *et al.* (2022)

5　结论

(1)锆石 LA-ICP-MS U-Pb 定年结果显示松辽盆地西缘突泉地区流纹岩结晶年龄为 156±1Ma,英云闪长玢岩结晶年龄为 155±1Ma, 表明其形成于晚侏罗世。

(2)晚侏罗世流纹岩和英云闪长玢岩具有过铝质 S 型花岗岩特征,其岩浆源区为加厚陆壳物质的部分熔融。

(3)蒙古-鄂霍茨克构造体系的影响范围到达了松辽盆地西缘突泉地区,研究区晚侏罗世流纹岩和英云闪长玢岩的形成与蒙古-鄂霍茨克洋洋壳俯冲和陆-陆碰撞有关,松辽盆地西缘及邻区在钦莫利阶(156±1Ma ~ 155±1Ma)处于蒙古-鄂霍茨克洋闭合到陆-陆碰撞转换阶段。

致谢　感谢吉林大学“火山岩储层及其油气藏地质-地球物理创新团队”在野外工作和锆石 U-Pb 测年分析中给予的大力帮助。感谢两位评审专家、责编和主编提出的宝贵意

见！这些意见对提高论文质量起到了重要作用！

References

Andersen T. 2002. Correction of common lead in U-Pb analyses that do not report ^{204}Pb. Chemical Geology, 192(1-2): 59-79

Barbarin B. 1996. Genesis of the two main types of peraluminous granitoids. Geology, 24(4): 295-298

Barbarin B. 1999. A review of the relationships between granitoid types, their origins and their geodynamic environments. Lithos, 46(3): 605-626

Batchelor RA and Bowden P. 1985. Petrogenetic interpretation of granitoid rock series using multicationic parameters. Chemical Geology, 48(1-4): 43-55

Boztuğ D, Harlavan Y, Arehart GB, Satır M and Avcı N. 2007. K-Ar age, whole-rock and isotope geochemistry of A-type granitoids in the Divriği-Sivas region, eastern-central Anatolia, Turkey. Lithos, 97(1-2): 193-218

Bureau of Geology and Mineral Resources of Jilin Province (BGMRJ). 1988. Regional Geology of Jilin Province. Beijing: Geological Publishing House, 365-367 (in Chinese)

Bussien D, Gombojav N, Winkler W and von Quadt A. 2011. The Mongol-Okhotsk Belt in Mongolia: An appraisal of the geodynamic development by the study of sandstone provenance and detrital zircons. Tectonophysics, 510(1-2): 132-150

Chappell BW and White AJR. 2001. Two contrasting granite types: 25 years later. Australian Journal of Earth Sciences, 48(4): 489-499

Chen L, Liang CY, Neubauer F, Liu YJ, Zhang Q and Song ZW. 2022. Sedimentary processes and deformation styles of the Mesozoic sedimentary succession in the northern margin of the Mohe basin, NE China: Constraints on the final closure of the Mongol-Okhotsk Ocean. Journal of Asian Earth Sciences, 232: 105052

Chen YX, Song SG, Niu YL and Wei CJ. 2014. Melting of continental crust during subduction initiation: A case study from the Chaidanuo peraluminous granite in the North Qilian suture zone. Geochimica et Cosmochimica Acta, 132: 311-336

Crawford AJ, Falloon TJ and Eggins S. 1987. The origin of island arc high-alumina basalts. Contributions to Mineralogy and Petrology, 97(3): 417-430

Deng JF, Zhao HL, Lai SC, Liu HX and Luo ZH. 1994. Generation of muscovite/two-mica granite and intracontinental subduction. Earth Science (Journal of China University of Geosciences), 19(2): 139-147 (in Chinese with English abstract)

Donskaya TV, Gladkochub DP, Mazukabzov AM and Ivanov AV. 2013. Late Paleozoic-Mesozoic subduction-related magmatism at the southern margin of the Siberian continent and the 150 million-year history of the Mongol-Okhotsk Ocean. Journal of Asian Earth Sciences, 62: 79-97

Eby GN. 1990. The A-type granitoids: A review of their occurrence and chemical characteristics and speculations on their petrogenesis. Lithos, 26(1-2): 115-134

Elburg MA. 1996. Genetic significance of multiple enclave types in a peraluminous ignimbrite suite, Lachlan Fold Belt, Australia. Journal of petrology, 37(6): 1385-1408

Enkin RJ, Yang ZY, Chen Y and Courtillot V. 1992. Paleomagnetic constraints on the geodynamic history of the major blocks of China from the Permian to the present. Journal of Geophysical Research: Solid Earth, 97(B10): 13953-13989

Finger F, Roberts MP, Haunschmid B, Schermaier A and Steyrer HP. 1997. Variscan granitoids of central Europe: Their typology, potential sources and tectonothermal relations. Mineralogy and Petrology, 61(1): 67-96

Gerdes A, Montero P, Bea F, Fershater G, Borodina N, Osipova T and Shardakova G. 2002. Peraluminous granites frequently with mantle-like isotope compositions: The continental-type Murzinka and Dzhabyk batholiths of the eastern Urals. International Journal of Earth Sciences, 91(1): 3-19

Guo F, Li HX, Fan WM, Li JY, Zhao L, Huang MW and Xu WL. 2015. Early Jurassic subduction of the Paleo-Pacific Ocean in NE China: Petrologic and geochemical evidence from the Tumen mafic intrusive complex. Lithos, 224-225: 46-60

Halim N, Kravchinsky V, Gilder S, Cogné JP, Alexyutin M, Sorokin A, Courtillot V and Chen Y. 1998. A palaeomagnetic study from the Mongol-Okhotsk region: Rotated Early Cretaceous volcanics and remagnetized Mesozoic sediments. Earth and Planetary Science Letters, 159(3-4): 133-145

Harris NBW, Pearce JA and Tindle AG. 1986. Geochemical characteristics of collision-zone magmatism. In: Coward MP and Reis AC (eds.). Collision Tectonics. Geological Society, London, Special Publications, 19(1): 67-81

He GQ, Liu C, Deng JF, Luo ZH, Zhang Y, Liu JX, Liu Q and Yue HJ. 2020. Records of the Late Jurassic magmatic arc in Heihe area, Heilongjiang Province: Discussion on the relationship with Mongolia-Okhotsk Ocean. Earth Science, 45(7): 2524-2537 (in Chinese with English abstract)

Hofmann AW, Jochum KP, Seufert M and White WM. 1986. Nb and Pb in oceanic basalts: New constraints on mantle evolution. Earth and Planetary Science Letters, 79(1-2): 33-45

Hoskin PWO and Schaltegger U. 2003. The composition of zircon and igneous and metamorphic petrogenesis. Reviews in Mineralogy and Geochemistry, 53(1): 27-62

Huang F, Zhang Z, Xu JF, Li XY, Zeng YC, Xu R, Liu XJ, Zhang LY, Zhang M, Yang CQ, Zhang LL, Yu HX and Yang XL. 2021. Lithospheric extension in response to subduction of the Paleo-Pacific Plate: Insights from Early Jurassic intraplate volcanic rocks in the Sk2 Borehole, Songliao Basin, NE China. Lithos, 380-381: 105871

Ji Z, Ge WC, Yang H, Wang QH, Zhang YL, Wang ZH and Bi JH. 2018. Late Jurassic rhyolites from the Wuchagou region in the central Great Xing'an Range, NE China: Petrogenesis and tectonic implications. Journal of Asian Earth Sciences, 158: 381-397

Ji Z, Meng QA, Wan CB, Zhu DF, Ge WC, Zhang YL, Yang H and Dong Y. 2019. Geodynamic evolution of flat-slab subduction of Paleo-Pacific Plate: Constraints from Jurassic Adakitic lavas in the Hailar Basin, NE China. Tectonics, 38(12): 4301-4319

Ji Z, Zhang YL, Wan CB, Ge WC, Yang H, Dong Y and Jing Y. 2021. Recycling of crustal materials and implications for lithospheric thinning: Evidence from Mesozoic volcanic rocks in the Hailar-Tamtsag Basin, NE China. Geoscience Frontiers, 12(5): 101184

Kapp JDA, Miller CF and Miller JS. 2002. Ireteba Pluton, Eldorado Mountains, Nevada: Late, deep-source, peraluminous magmatism in the Cordilleran Interior. The Journal of Geology, 110(6): 649-669

Kimura JI and Nagahashi Y. 2007. Origin of a voluminous iron-enriched high-K rhyolite magma erupted in the North Japan Alps at 1.75Ma: Evidence for upper crustal melting. Journal of Volcanology and Geothermal Research, 167(1-4): 81-99

Kirillova GL. 2003. Late Mesozoic-Cenozoic sedimentary basins of active continental margin of Southeast Russia: Paleogeography, tectonics and coal-oil-gas presence. Marine and Petroleum Geology, 20(3-4): 385-397

Kravchinsky VA, Cogné JP, Harbert WP and Kuzmin MI. 2002. Evolution of the Mongol-Okhotsk Ocean as constrained by new palaeomagnetic data from the Mongol-Okhotsk suture zone, Siberia. Geophysical Journal International, 148(1): 34-57

Le Fort P, Cuney M, Deniel C, France-Lanord C, Sheppard SMF, Upreti BN and Vidal P. 1987. Crustal generation of the Himalayan leucogranites. Tectonophysics, 134(1-3): 39-57

Li JY, He ZJ, Mo SG and Zheng QD. 1999. The Late Mesozoic orogenic processes of Mongolia-Okhotsk Orogen: Evidence from field investigations into deformation of the Mohe area, NE China. Journal of Geoscientific Research in Northeast Asia, 2(2): 172-178

Li Y, Ding LL, Xu WL, Wang F, Tang J, Zhao S and Wang ZJ. 2015. Geochronology and geochemistry of muscovite granite in Sunwu area,

NE China: Implications for the timing of closure of the Mongol-Okhotsk Ocean. Acta Petrologica Sinica, 31(1): 56 – 66 (in Chinese with English abstract)

Li Y, Xu WL, Wang F, Pei FP, Tang J and Zhao S. 2017. Triassic volcanism along the eastern margin of the Xing'an Massif, NE China: Constraints on the spatial-temporal extent of the Mongol-Okhotsk tectonic regime. Gondwana Research, 48: 205 – 223

Liu CF, Zhou ZG, Wang GS, Wu C, Li HY, Zhu Y, Jiang T, Liu WC and Ye BY. 2018. Geochronology and geochemistry of the Late Jurassic bimodal volcanic rocks from Hailisen area, central-southern Great Xing'an Range, Northeast China. Geological Journal, 53(5): 2099 – 2117

Liu CY, Shan XL, Yi J, Ren XJ, Han JY, Niu PH and Xing J. 2022. Volcanism from different eruption cycles during the Early Cretaceous in the Changling fault depression of the Songliao Basin, NE China, and their implications for timing of lithospheric thinning. International Geology Review, 64(4): 509 – 529

Liu YJ, Li WM, Feng ZQ, Wen QB, Neubauer F and Liang CY. 2017. A review of the Paleozoic tectonics in the eastern part of Central Asian Orogenic Belt. Gondwana Research, 43: 123 – 148

Liu YS, Gao S, Hu ZC, Gao CG, Zong KQ and Wang DB. 2010. Continental and oceanic crust recycling-induced melt-peridotite interactions in the Trans-North China Orogen: U-Pb dating, Hf isotopes and trace elements in zircons from mantle xenoliths. Journal of Petrology, 51(1 – 2): 537 – 571

Ludwig KR. 2003. User's Manual for ISOPLOT 3. 00: A Geochronological Toolkit for Microsoft Excel. Berkeley: Berkeley Geochronology Center, 4: 74

Maniar PD and Piccoli PM. 1989. Tectonic discrimination of granitoids. GSA Bulletin, 101(5): 635 – 643

Maruyama S, Isozaki Y, Kimura G and Terabayashi M. 1997. Paleogeographic maps of the Japanese Islands: PLATE tectonic synthesis from 750Ma to the present. Island Arc, 6(1): 121 – 142

Meng QR. 2003. What drove late Mesozoic extension of the northern China-Mongolia tract? Tectonophysics, 369(3 – 4): 155 – 174

Metelkin DV, Gordienko IV and Klimuk VS. 2007. Paleomagnetism of Upper Jurassic basalts from Transbaikalia: New data on the time of closure of the Mongol-Okhotsk Ocean and Mesozoic intraplate tectonics of Central Asia. Russian Geology and Geophysics, 48(10): 825 – 834

Metelkin DV, Vernikovsky VA, Kazansky AY and Wingate MTD. 2010. Late Mesozoic tectonics of Central Asia based on paleomagnetic evidence. Gondwana Research, 18(2 – 3): 400 – 419

Middlemost EAK. 1994. Naming materials in the magma/igneous rock system. Earth-Science Reviews, 37(3 – 4): 215 – 224

Miller CF, McDowell SM and Mapes RW. 2003. Hot and cold granites? Implications of zircon saturation temperatures and preservation of inheritance. Geology, 31(6): 529 – 532

Mo XX, Hou ZQ, Niu YL, Dong GC, Qu XM, Zhao ZD and Yang ZM. 2007. Mantle contributions to crustal thickening during continental collision: Evidence from Cenozoic igneous rocks in southern Tibet. Lithos, 96(1 – 2): 225 – 242

Ouyang HG, Mao JW, Zhou ZH and Su HM. 2015. Late Mesozoic metallogeny and intracontinental magmatism, southern Great Xing'an Range, northeastern China. Gondwana Research, 27(3): 1153 – 1172

Oxman VS. 2003. Tectonic evolution of the Mesozoic Verkhoyansk-Kolyma belt (NE Asia). Tectonophysics, 365(1 – 4): 45 – 76

Parfenov LM, Popeko LI and Tomurtogoo O. 2001. Problems of tectonics of the Mongol-Okhotsk orogenic belt. Geology of the Pacific Ocean, 16(5): 797 – 830

Parfenov LM, Berzin NA, Khanchuk AI, Badarch G, Belichenko VG, Bulgatov AN, Dril SI, Kirillova GL, Kuzmin MI, Nokleberg WJ, Prokopyev AV, Timofeev VF, Tomurtogoo O and Yang H. 2003. A model for the formation of orogenic belts in Central and Northeast Asia. Tikhookeanskaya Geologiya, 22(6): 7 – 41 (in Russian)

Patiño Douce AE and Johnston AD. 1991. Phase equilibria and melt productivity in the pelitic system: Implications for the origin of peraluminous granitoids and aluminous granulites. Contributions to Mineralogy and Petrology, 107(2): 202 – 218

Pearce JA. 1983. Role of the sub-continental lithosphere in magma genesis at active continental margins. In: Hawkesworth CJ and Norry MJ (eds.). Continental Basalts and Mantle Xenoliths. Nantwich: Shiva Publishing, 230 – 249

Pearce JA, Harris NBW and Tindle AG. 1984. Trace element discrimination diagrams for the tectonic interpretation of granitic rocks. Journal of Petrology, 25(4): 956 – 983

Pearce JA, Bender JF, De Long SE, Kidd WSF, Low PJ, Güner Y, Saroglu F, Yilmaz Y, Moorbath S and Mitchell JG. 1990. Genesis of collision volcanism in Eastern Anatolia, Turkey. Journal of Volcanology and Geothermal Research, 44(1 – 2): 189 – 229

Peccerillo A and Taylor SR. 1976. Geochemistry of Eocene calc-alkaline volcanic rocks from the Kastamonu area, Northern Turkey. Contributions to Mineralogy and Petrology, 58(1): 63 – 81

Profeta L, Ducea MN, Chapman JB, Paterson SR, Gonzales SMH, Kirsch M, Petrescu L and DeCelles PG. 2015. Quantifying crustal thickness over time in magmatic arcs. Scientific Reports, 5(1): 17786

Ren Q, Zhang SH, Wu HC, Liang ZK, Miao XJ, Zhao HQ, Li HY, Yang TS, Pei JL and Davis GA. 2016. Further paleomagnetic results from the ~ 155Ma Tiaojishan Formation, Yanshan Belt, North China, and their implications for the tectonic evolution of the Mongol-Okhotsk suture. Gondwana Research, 35: 180 – 191

Rudnick RL and Fountain DM. 1995. Nature and composition of the continental crust: A lower crustal perspective. Reviews of Geophysics, 33(3): 267 – 309

Schärer U, Xu RH and Allègre CJ. 1986. U-(Th)-Pb systematics and ages of Himalayan leucogranites, South Tibet. Earth and Planetary Science Letters, 77(1): 35 – 48

Searle MP, Parrish RR, Hodges KV, Hurford A, Ayres MW and Whitehouse MJ. 1997. Shisha Pangma Leucogranite, South Tibetan Himalaya: Field relations, geochemistry, age, origin, and emplacement. The Journal of Geology, 105(3): 295 – 318

Şengör AMC and Natal'in BA. 1996. Paleotectonics of Asia: Fragments of a synthesis. In: Yin A and Harrison TM (eds.). The Tectonic Evolution of Asia. Cambridge: Cambridge University Press, 486 – 641

Shi L, Tang Z, Zheng CQ, Qin T, Zhang LD, Wang Y, Qian C and Yang F. 2020. Genesis and tectonic significance of Late Jurassic Granitoids in Chaihe Region, Central Great Xing'an Range, NE China. Journal of Jilin University (Earth Science Edition), 50(1): 112 – 128 (in Chinese with English abstract)

Sun DY, Gou J, Wang TH, Ren YS, Liu YJ, Guo HY, Liu XM and Hu ZC. 2013. Geochronological and geochemical constraints on the Erguna massif basement, NE China: Subduction history of the Mongol-Okhotsk oceanic crust. International Geology Review, 55(14): 1801 – 1816

Sun SS and McDonough WF. 1989. Chemical and isotopic systematics of oceanic basalts: Implications for mantle composition and processes. In: Saunders AD and Norry MJ (eds.). Magmatism in the Ocean Basins. Geological Society, London, Special Publication, 42(1): 313 – 345

Sylvester PJ. 1998. Post-collisional strongly peraluminous granites. Lithos, 45(1 – 4): 29 – 44

Tang J, Xu WL, Wang F, Zhao S and Li Y. 2015. Geochronology, geochemistry, and deformation history of Late Jurassic-Early Cretaceous intrusive rocks in the Erguna Massif, NE China: Constraints on the late Mesozoic tectonic evolution of the Mongol-Okhotsk orogenic belt. Tectonophysics, 658: 91 – 110

Tang J, Xu WL, Wang F, Zhao S and Wang W. 2016. Early Mesozoic southward subduction history of the Mongol-Okhotsk oceanic plate: Evidence from geochronology and geochemistry of Early Mesozoic intrusive rocks in the Erguna Massif, NE China. Gondwana Research, 31: 218 – 240

Tang ZY, Sun DY, Mao AQ, Yang DG and Deng CZ. 2019. Timing and evolution of Mesozoic volcanism in the central Great Xing'an Range,

northeastern China. Geological Journal, 54(6): 3737 – 3754
Tomurtogoo O, Windley BF, Kröner A, Badarch G and Liu DY. 2005. Zircon age and occurrence of the Adaatsag ophiolite and Muron shear zone, central Mongolia: Constraints on the evolution of the Mongol-Okhotsk Ocean, suture and orogen. Journal of the Geological Society, 162(1): 125 – 134
von Blanckenburg F. 1992. Combined high-precision chronometry and geochemical tracing using accessory minerals: Applied to the Central-Alpine Bergell intrusion (central Europe). Chemical Geology, 100(1 – 2): 19 – 40
Wang F, Zhou XH, Zhang LC, Ying JF, Zhang YT, Wu FY and Zhu RX. 2006. Late Mesozoic volcanism in the Great Xing'an Range (NE China): Timing and implications for the dynamic setting of NE Asia. Earth and Planetary Science Letters, 251(1 – 2): 179 – 198
Wang F, Xu WL, Xing KC, Wang YN, Zhang HH, Wu W, Sun CY and Ge WC. 2019. Final closure of the Paleo-Asian Ocean and onset of subduction of Paleo-Pacific Ocean: Constraints from Early Mesozoic magmatism in central southern Jilin Province, NE China. Journal of Geophysical Research: Solid Earth, 124(3): 2601 – 2622
Wang PJ, Mattern F, Didenko NA, Zhu DF, Singer B and Sun XM. 2016. Tectonics and cycle system of the Cretaceous Songliao Basin: An inverted active continental margin basin. Earth-Science Reviews, 159: 82 – 102
Wang W, Tang J, Xu WL and Wang F. 2015. Geochronology and geochemistry of Early Jurassic volcanic rocks in the Erguna Massif, Northeast China: Petrogenesis and implications for the tectonic evolution of the Mongol-Okhotsk suture belt. Lithos, 218 – 219: 73 – 86
Watson EB and Capobianco CJ. 1981. Phosphorus and the rare earth elements in felsic magmas: An assessment of the role of apatite. Geochimica et Cosmochimica Acta, 45(12): 2349 – 2358
Whalen JB, Currie KL and Chappell BW. 1987. A-type granites: Geochemical characteristics, discrimination and petrogenesis. Contributions to Mineralogy and Petrology, 95(4): 407 – 419
White AJR and Chappell BW. 1977. Ultra-metamorphism and granitoid genesis. Tectonophysics, 43(1 – 2): 7 – 22
White AJR and Chappell BW. 1988. Some supracrustal (S-type) granites of the Lachlan Fold Belt. Earth and Environmental Science Transactions of the Royal Society of Edinburgh, 79(2 – 3): 169 – 181
Wu FY, Sun DY, Li HM, Jahn BM and Wilde S. 2002. A-type granites in northeastern China: Age and geochemical constraints on their petrogenesis. Chemical Geology, 187(1 – 2): 143 – 173
Wu FY, Sun DY, Ge WC, Zhang YB, Grant ML, Wilde SA and Jahn BM. 2011. Geochronology of the Phanerozoic granitoids in northeastern China. Journal of Asian Earth Sciences, 41(1): 1 – 30
Wu G, Chen YJ, Sun FY, Li JC, Li ZT and Wang XJ. 2008. Geochemistry of the Late Jurassic Granitoids in the northern end area of Da Hinggan Mountains and their geological and prospecting implications. Acta Petrologica Sinica, 24(4): 899 – 910 (in Chinese with English abstract)
Xu J, Xia XP, Wang Q, Spencer CJ, Lai CK, Ma JL, Zhang L, Cui ZX, Zhang WF and Zhang YQ. 2022. Pure sediment-derived granites in a subduction zone. GSA Bulletin, 134(3 – 4): 599 – 615
Xu WL, Pei FP, Wang F, Meng E, Ji WQ, Yang DB and Wang W. 2013. Spatial-temporal relationships of Mesozoic volcanic rocks in NE China: Constraints on tectonic overprinting and transformations between multiple tectonic regimes. Journal of Asian Earth Sciences, 74: 167 – 193
Yang QD, Guo L, Wang T, Zeng T, Zhang L, Tong Y, Shi XJ and Zhang JJ. 2014. Geochronology, origin, sources and tectonic settings of Late Mesozoic two-stage granites in the Ganzhuermiao region, central and southern Da Hinggan Range, NE China. Acta Petrologica Sinica, 30(7): 1961 – 1981 (in Chinese with English abstract)
Yang YT, Guo ZX, Song CC, Li XB and He S. 2015. A short-lived but significant Mongol-Okhotsk collisional orogeny in latest Jurassic-earliest Cretaceous. Gondwana Research, 28(3): 1096 – 1116
Yin ZG, Gong ZM, Zhang YL, Cao ZQ, Li M, Li HN, Wang Y, Han Y and Zhang ST. 2018. LA-ICP-MS zircon U-Pb dating and geochemical characteristics of the Late Jurassic monzonitic granite from Yilehuli Mountain in northern Da Hinggan Mountains and their geological implications. Geological Bulletin of China, 37(7): 1291 – 1301 (in Chinese with English abstract)
Yin ZG, Hao K, Liu CL, Wang Y, Li HN, Li M, Gong ZM and Zhang ST. 2019. Geochronological and geochemical characteristics of rhyolite in the Manketou'ebo Formation of Dong Ujimqin Banner, Inner Mongolia, and its geological implications. Geological Bulletin of China, 38(11): 1825 – 1835 (in Chinese with English abstract)
Yu TJ, Wang PJ, Zhang Y, Gao YF and Chen CC. 2022. Discovery of the Late Jurassic-Early Cretaceous lamprophyres in western Songliao basin of Northeast China and their constraint on regional lithospheric evolution. Frontiers in Earth Science, 10: 849665
Yu TJ. 2023. Late Mesozoic magmatism and sedimentation in the Tuquan area along the western margin of the Songliao Basin: Implications for regional tectonics. Ph. D. Dissertation. Changchun: Jilin University (in Chinese with English abstract)
Zhang C, Zhang YJ, Quan JY, Guo W, Guo JG, Wang QZ, Li W, Wang Y, Song WM, Na FC and Tan HY. 2018. Zircon U-Pb geochronology and petrogenesis of rhyolites in Manketouebo Formation from the Kundu area in Jarud Basin, Inner Mongolia. Geological Bulletin of China, 37(9): 1633 – 1643 (in Chinese with English abstract)
Zhang C, Quan JY, Zhang YJ, Liu ZH, Li W, Wang Y, Qian C, Zhang L and Ge JT. 2020. Late Mesozoic tectonic evolution of the southern Great Xing'an Range, NE China: Evidence from whole-rock geochemistry, and zircon U-Pb ages and Hf isotopes from volcanic rocks. Lithos, 362 – 363: 105409
Zhang FQ, Chen HL, Yu X, Dong CW, Yang SF, Pang YM and Batt GE. 2011. Early Cretaceous volcanism in the northern Songliao Basin, NE China, and its geodynamic implication. Gondwana Research, 19(1): 163 – 176
Zhang HF, Harris N, Parrish R, Zhang L, Zhao ZD and Li DW. 2005. Geochemistry of North Himalayan leucogranites: Regional comparison, petrogenesis and tectonic implications. Earth Science, 30(3): 275 – 288 (in Chinese with English abstract)
Zhang JH, Gao S, Ge WC, Wu FY, Yang JH, Wilde SA and Li M. 2010. Geochronology of the Mesozoic volcanic rocks in the Great Xing'an Range, northeastern China: Implications for subduction-induced delamination. Chemical Geology, 276(3 – 4): 144 – 165
Zhang JH, Ge WC, Wu FY, Wilde SA, Yang JH and Liu XM. 2008. Large-scale Early Cretaceous volcanic events in the northern Great Xing'an Range, northeastern China. Lithos, 102(1 – 2): 138 – 157
Zhang Q, Wang YL, Jin WJ, Jia XQ and Li CD. 2008. Criteria for the recognition of pre-, syn- and post-orogenic granitic rocks. Geological Bulletin of China, 27(1): 1 – 18 (in Chinese with English abstract)
Zhang Q, Jin WJ, Li CD, Wang Y and Wang YL. 2011. Granitic rocks and their formation depth in the crust. Geotectonica et Metallogenia, 35(2): 259 – 269 (in Chinese with English abstract)
Zhao Y, Yang ZY and Ma XH. 1994. Geotectonic transition from Paleo-Asian system and Paleo-Tethyan system to Paleo-Pacific active continental margin in eastern Asia. Chinese Journal of Geology, 29(2): 105 – 119 (in Chinese with English abstract)
Zhao YD, Che JY, Xu FM, Zhu Q and Wang KL. 2018. Late Jurassic adakitic granites in northeastern Xing'an block: Geochronology and geochemical characteristics and tectonic significance. Earth Science Frontiers, 25(6): 240 – 253 (in Chinese with English abstract)
Zorin YA. 1999. Geodynamics of the western part of the Mongolia-Okhotsk collisional belt, Trans-Baikal region (Russia) and Mongolia. Tectonophysics, 306(1): 33 – 56

附中文参考文献

邓晋福, 赵海玲, 赖绍聪, 刘厚祥, 罗照华. 1994. 白云母/二云母花

岗岩形成与陆内俯冲作用. 地球科学, 19(2): 139 – 147

贺国奇, 刘翠, 邓晋福, 罗照华, 张昱, 刘继旭, 刘庆, 岳洪举, 2020. 黑龙江黑河地区晚侏罗世岩浆弧的火成岩记录: 与蒙古-鄂霍茨克洋关系探讨. 地球科学, 45(7): 2524 – 2537

吉林省地质矿产局. 1988. 吉林省区域地质志. 北京: 地质出版社, 365 – 367

李宇, 丁磊磊, 许文良, 王枫, 唐杰, 赵硕, 王子进. 2015. 孙吴地区中侏罗世白云母花岗岩的年代学与地球化学: 对蒙古-鄂霍茨克洋闭合时间的限定. 岩石学报, 31(1): 56 – 66

施璐, 唐振, 郑常青, 秦涛, 张立东, 汪岩, 钱程, 杨帆. 2020. 大兴安岭中部柴河地区晚侏罗世花岗质岩石成因及构造意义. 吉林大学学报(地球科学版), 50(1): 112 – 128

武广, 陈衍景, 孙丰月, 李景春, 李之彤, 王希今. 2008. 大兴安岭北端晚侏罗世花岗岩类地球化学及其地质和找矿意义. 岩石学报, 24(4): 899 – 910

杨奇荻, 郭磊, 王涛, 曾涛, 张磊, 童英, 史兴俊, 张建军. 2014. 大兴安岭中南段甘珠尔庙地区晚中生代两期花岗岩的时代、成因、物源及其构造背景. 岩石学报, 30(7): 1961 – 1981

尹志刚, 宫兆民, 张跃龙, 曹忠强, 李敏, 李海娜, 王阳, 韩宇, 张圣听. 2018. 大兴安岭北段伊勒呼里山晚侏罗世二长花岗岩 LA-ICP-MS 锆石 U-Pb 年龄、地球化学特征及其地质意义. 地质通报, 37(7): 1291 – 1301

尹志刚, 郝科, 刘成龙, 王阳, 李海娜, 李敏, 宫兆民, 张圣听. 2019. 内蒙古东乌旗地区满克头鄂博组流纹岩年代学、地球化学特征及其地质意义. 地质通报, 38(11): 1825 – 1835

于太极. 2023. 松辽盆地西缘突泉地区晚中生代岩浆作用和沉积特征及其区域构造意义. 博士学位论文. 长春: 吉林大学

张超, 张渝金, 权京玉, 郭威, 郭建刚, 王青召, 李伟, 汪岩, 宋维民, 那福超, 谭红艳. 2018. 内蒙古扎鲁特盆地坤都地区满克头鄂博组流纹岩锆石 U-Pb 年龄及岩石成因. 地质通报, 37(9): 1633 – 1643

张宏飞, Harris N, Parrish R, 张利, 赵志丹, 李德威. 2005. 北喜马拉雅淡色花岗岩地球化学: 区域对比、岩石成因及其构造意义. 地球科学, 30(3): 275 – 288

张旗, 王元龙, 金惟俊, 贾秀勤, 李承东. 2008. 造山前、造山和造山后花岗岩的识别. 地质通报, 27(1): 1 – 18

张旗, 金惟俊, 李承东, 王焰, 王元龙. 2011. 花岗岩与地壳厚度关系探讨. 大地构造与成矿学, 35(2): 259 – 269

赵院冬, 车继英, 许逢明, 朱群, 王奎良. 2018. 兴安地块东北部晚侏罗世 C 型埃达克质花岗岩年代学、地球化学特征及构造环境意义. 地学前缘, 25(6): 240 – 253

赵越, 杨振宇, 马醒华. 1994. 东亚大地构造发展的重要转折. 地质科学, 29(2): 105 – 119